

**USING ISENTROPIC TECHNIQUES TO IMPROVE THE
UTILITY OF GOES MOISTURE OBSERVATIONS**

by

William E. Line

A thesis submitted in partial fulfillment of
the requirements for the degree of

Master of Science

(Atmospheric and Oceanic Sciences)

at the

UNIVERSITY OF WISCONSIN-MADISON

2013

Abstract

Although Geostationary Operational Environmental Satellite (GOES) sounding observations of moisture are unique in their ability to depict the pre-convective environment at high temporal and spatial resolutions in three-dimensions, new approaches are needed to more fully take advantage of this highly under-utilized dataset. The NearCast model is a Lagrangian trajectory model that has been developed to take advantage of the GOES temperature and moisture retrieval data by dynamically projecting every observation forward in space and time to improve 1-9 hour forecasts of hazardous weather. The model is run at multiple levels of the atmosphere so deep-layer atmospheric stability and shear can be computed, helping to improve short-term predictions of the timing and location of convection. By using a Lagrangian framework, the model preserves fine details in the observations such as minima, maxima, and boundaries while providing output to forecasters shortly after the observations are made by the GOES sounder.

Because the temperature and moisture retrievals are made from the clear sky where flow is mostly adiabatic, an isentropic approach provides a better framework to predict their movement, as opposed to the isobaric system used in the original version of the model. Accordingly, an isentropic version of the NearCast model has been developed that computes parcel trajectories in three-dimensions along constant potential temperature surfaces. In addition to providing more accurate and detailed stability and shear information, the isentropic NearCast model depicts adiabatic lift and total isentropic layer moisture, further narrowing down when and where convection is most and least likely to occur. By identifying the total moisture content within an isentropic layer, predictions can also be made about the intensity of precipitation that will take place once convection occurs.

Contents

1	Introduction	1
2	Background	7
2.1	Early History of the Isentropic Vertical Coordinate	7
2.2	Atmospheric Trajectories	10
2.3	Isentropic Coordinates in NWP	14
2.4	Advantages of Isentropic Analysis	15
2.5	Shortcomings of Isentropic Analysis	16
3	Data	17
3.1	Temperature and Moisture Observations	17
3.2	Wind and Mass Field Data	21
4	Methods	21
5	Results	26
5.1	April 09, 2011-Isobaric NearCast	27
5.2	April 09, 2011-Isentropic NearCast	40
5.3	June 08, 2011 - Isentropic NearCast	55
5.4	June 01, 2011 and May 29, 2012 - Isentropic NearCast	60
6	Summary and Conclusions	69

List of Figures

- | | | |
|---|--|----|
| 1 | 2010-2012 monthly averages of National Centers for Environmental Prediction (NCEP) Global Forecast System (GFS) and North American Mesoscale Model (NAM) 3-hourly precipitation forecast threat scores. Equitable threat scores are a measure of the model forecast accuracy, where lower scores indicate lower precipitation forecast accuracy when compared to what was observed. Data obtained from the NCEP/EMC webpage. | 2 |
| 2 | Back trajectories computed along the 295, 300, and 305 K isentropic surfaces in the vicinity of the April 23, 1963 tornado outbreak. Analysis in text. From Danielsen (1964). | 12 |
| 3 | 2011 monthly comparisons of Global Positioning System (GPS) total precipitable water (TPW) measurements with GOES TPW (Li retrievals) and GFS first guess TPW. Standard deviations (Std Dev) were calculated wherever there was a collocation of a GPS site and a GOES retrieval. Analysis in text. From Petersen <i>et al.</i> (2012). | 20 |

4	Graphical depiction of how the NearCast model uses up to 10 hours of old observations from previous model forecasts in its current analysis and forecast display products to fill in data void area. Output from every forecast hour in the column above a given analysis or forecast hour is used in that analysis or forecast display. Detailed explanation of this process in text.	25
5	3-hourly sequence of 10.7 μm imagery measured by the GOES-East imager on April 09-10 2011.	27
6	Storm Prediction Center (SPC) severe storm reports for April 09, 2011 (the 24 hour period ending 1200 UTC on April 10, 2011). Inset is observed precipitation for the same period, obtained from the National Weather Service (NWS) Advanced Hydrologic Prediction Service.	28

7	1500 UTC April 09, 2011 isobaric NearCast model cycle. Analysis and forecast displays use the most recent (1500 UTC) observations from the GOES sounder, as well as previous model cycle trajectories from as far back as 0500 UTC. Upper level is 500 hPa, lower level is 780 hPa, and θ_e difference is upper-level minus lower-level θ_e . Colorbar on left represents θ_e . Higher (lower) values indicate warm and moist (dry and cool) air. Colorbar on right is θ_e difference. Negative (positive) values indicate the layer is convectively unstable (stable). Winds are in knots. White areas are where no retrievals were made (or projected into) due to the presence of cloud cover. Black contours in θ_e difference plots are θ_e difference 2 hour time tendencies, starting at -6K/2 hr, decreasing by 3 K increments. More contours (more negative values) signify more rapid destabilization.	32
8	Same as Fig. 7, but for 1800 UTC.	35
9	Same as Fig. 7, but for 2100 UTC.	37
10	Comparisons of convective instability between the 1500, 1800, and 2100 UTC NearCast forecasts valid at 2100 and 0000 UTC on April 09, 2011.	39
11	1500 UTC April 09, 2011 isentropic NearCast model cycle. Similar to Fig. 7, but with trajectories along constant isentropic surfaces as opposed to isobaric ones. Upper level is 318 K , lower level is 312 K, red contours are pressure in hPa. See text for details.	42

12	1500 UTC April 09, 2011 isentropic NearCast model cycle. Adiabatic vertical motion and its two components along the lower (312 K) isentropic surface. Left (right) colorbar is upward (downward) vertical motion. Higher values indicate more rapid vertical motion. Units are $\mu\text{bar/s}$. Interpretation in text.	46
13	1500 UTC April 09, 2011 isentropic NearCast model cycle. Average mixing ratio ($\frac{g}{kg}$), layer mass ($\frac{kg}{Km^2}$), and layer moisture ($\frac{gmoisture}{Km^2}$) within the lower (312 K) isentropic layer. Interpretation in text.	49
14	Same as Fig. 11, but for 2100 UTC.	51
15	Same as Fig. 12, but for 2100 UTC.	52
16	Same as Fig. 13, but for 2100 UTC.	53
17	Same as Fig. 5, but for June 08, 2011.	56
18	Same as Fig. 6, but for June 08, 2011.	57
19	Same as Fig. 11, but for 2100 UTC June 08, 2011. Upper level is 320 K, lower level is 312 K.	58
20	Same as Fig. 13, but for 2100 UTC June 08, 2011. Upper level is 320 K, lower level is 312 K.	59
21	Same as Fig. 5, but for June 01, 2011.	61
22	Same as Fig. 6, but for June 01, 2011.	62
23	Same as Fig. 11, but for 1500 UTC June 01, 2011. Upper level is 320 K, lower level is 310 K.	63

24	Same as Fig. 13, but for 1500 UTC June 01, 2011. Upper level is 320 K, lower level is 310 K.	64
25	Same as Fig. 5, but for May 29, 2012.	65
26	Same as Fig. 6, but for May 29, 2012.	66
27	Same as Fig. 11, but for 1500 UTC May 29, 2012. Upper level is 318 K, lower level is 308 K.	67
28	Same as Fig. 13, but for 1500 UTC May 29, 2012. Upper level is 318 K, lower level is 308 K.	68

1 Introduction

Despite continued improvements in Numerical Weather Prediction (NWP), precipitation and disruptive weather forecast accuracy in the short-range (3-12 hour) still needs substantial improvement by forecasters, especially in the summer months (Fig. 1). Part of this reduced skill is due to the inability of current NWP products to capture and predict mesoscale moisture features accurately. More specifically, forecasting summertime convection from the clear sky is a difficult task using current NWP products and nowcasting methods. Satellite observations can help meteorologists improve such forecasts.

Explorer 7 was the first meteorological satellite, taking the first measurements of radiation emitted from Earth in 1959 (Library, cited 2013). By 1966, the first geostationary satellite (ATS-1) was in orbit taking the first continuous measurements of Earth from space. 1975 marked the launch of GOES 1, the first satellite in the current Geostationary Operational Environmental Satellite (GOES) program. Europeans provided the earliest water vapor images in the late 1970s with Meteosat, utilizing the $6.7 \mu m$ wavelength to observe the movement of mid- to upper-level tropospheric moisture. The multispectral satellite imagery provided new visual evidence of atmospheric processes at work, proving to be especially useful in observing the movement of upper-level moisture and dryness features. One of the processes that water vapor imagery captured was the formation of convection along the leading edge of upper-level dry air streaks as they overlay areas of low-level moisture.

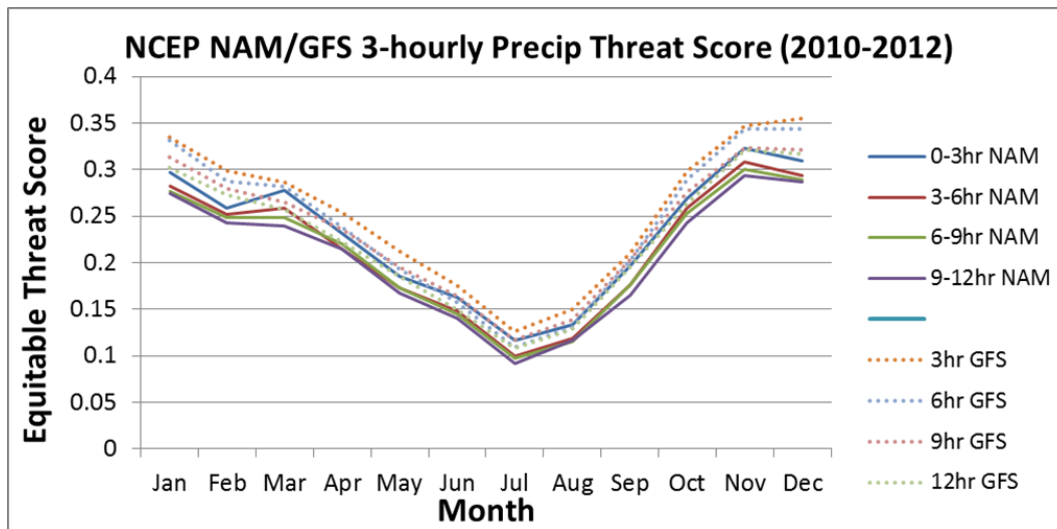


Figure 1: 2010-2012 monthly averages of National Centers for Environmental Prediction (NCEP) Global Forecast System (GFS) and North American Mesoscale Model (NAM) 3-hourly precipitation forecast threat scores. Equitable threat scores are a measure of the model forecast accuracy, where lower scores indicate lower precipitation forecast accuracy when compared to what was observed. Data obtained from the NCEP/EMC webpage.

In 1980, VAS (Visible Infrared Spin Scan Radiometer (VISSR) Atmospheric Sounder) was launched into orbit aboard GOES 4, becoming the first device to take continuous vertical soundings of temperature and moisture through the atmosphere. The sounder consisted of 12 Infrared (IR) channels, and was flown aboard GOES 4-7. In 1994, the GOES sounder was enhanced to include 18 IR channels on a 3-axis stabilized sounder, which was flown on GOES 8-15.

A physical retrieval process takes information from the GOES sounder to adjust model first guess profiles to produce updated profiles of temperature and moisture, or retrievals. Since these observations are made from the clear sky, they represent the only dataset to provide detailed multi-layer information about the pre-convective environment over the continental United States (CONUS) at high spatial and temporal

resolutions, quantifying what the moisture imagery had been showing. Having such high resolution measurements of temperature and moisture in four dimensions is useful in determining atmospheric stability and, therefore, where convection is most and least likely to occur. These observations are especially valuable in depicting trends in the moisture fields and fine details such as boundaries, maxima and minima. A problem remains, however, as to how to include these data in objective forecast tools.

Despite over 30 years of having such information-rich profiles, the GOES retrievals remain a highly under-utilized dataset. None of the current NWP models assimilate clear sky GOES moisture observations over land for several reasons. For one, biases stemming from the model first guess can lead to errors in the final retrieval products. Also, the high land surface emissivity can introduce errors, making it difficult to use the retrievals over land.

In addition to the aforementioned problems, other issues would limit the utility of real-time, high resolution GOES moisture data in numerical models. All operational NWP models used today are Eulerian, which predict changes in variables at fixed points (or grid points) through time. The initial value of a variable at each grid point is the result of a complex statistical combination of all observations near each grid point, a process which smooths maxima, minima and extreme gradients. Equations of motion are then used to determine how each variable will change in value over time at each grid point. In order to preserve the full resolution (~ 10 km) GOES observations, a fine mesh model resolution would be required. This, in turn, necessitates a small time step (10-15 seconds) to assure computational stability, which leads to long model run

times. Consequently, model output valid during the first several hours of the forecasts are not distributed in time for forecasters to use. Furthermore, because most models only update every six hours, forecasters are often forced to use model results that come from observations that are 9-10 hours old.

On the other hand, larger grid spacing (coarser resolution) could allow for longer time steps to be used, leading to quicker run times. These models, however, would smooth the data even further. Efforts to improve short-range forecasts in NWP have been made with the development of the Rapid Update Cycle (RUC) model, now Rapid Refresh (RAP). Still, these models share many of the same characteristics and problems associated with traditional NWP, and do not use GOES sounder data over land.

Although satellite sounding observations of moisture will likely someday be important in improving the accuracy of NWP short-term precipitation forecasts, an alternative method of using the GOES retrieval data has been developed at the Cooperative Institute for Meteorological Satellite Studies (CIMSS). The CIMSS NearCast model is a quick-updating and simple solution that uses the under-utilized satellite moisture observations and extends their use into forecasts of the pre-convective environment. The model takes advantage of what satellites observe best (the movement of moisture through the atmosphere in three-dimensions) to help improve the short-term prediction of precipitation and hazardous weather. It is especially valuable when used in conjunction with other forecaster tools, such as NWP. The GOES moisture data are being used in a way that has never been done to improve the situational awareness of heavy precipitation and hazardous weather by taking advantage of what satellites have shown

for decades: convection tends to form on the leading edge of upper-level dryness as it moves over areas of low-level moisture.

The NearCast model is a Lagrangian trajectory model that dynamically projects satellite temperature and moisture retrieval data forward in space and time at multiple levels of the atmosphere. The technique preserves fine details present in the full-resolution observations. Multi-level output can be used to determine where and when convective development is most (and least) likely in the near future (1-9 hour forecast range). The model is also helpful when making predictions about the environment into which already developed convection is moving, and whether or not that environment will support further convective growth. By merging ten hours of previous observations in its analysis and forecast products, the NearCast model is able to provide stability information in areas even after the IR satellite observations become cloud contaminated.

In a Lagrangian framework, every GOES observation can be tracked at full resolution as it moves through space and time. This approach can use a much larger time step (10-15 minutes) since the highly non-linear advective terms are not included in the equations of motion. The use of a large time step results in comparatively quick run times (minutes instead of hours) leading to little latency in the model output. Because the model updates whenever new observations become available, forecasters are able to have the most up to date information at hand. Finally, since there is no averaging of data over a grid, moisture boundaries, maxima, and minima are preserved, leading to detailed forecasts of atmospheric stability.

Although the errors and biases that exist in the absolute values of the retrievals can

severely disrupt more complex NWP models, they are not of much concern in this simple transport model. Analysis of the model output instead focuses on the relative values between atmospheric layers and on the horizontal distribution of moisture throughout the atmosphere.

The model's original configuration is in isobaric coordinates, meaning trajectories are made along constant pressure surfaces. This configuration has been shown to perform quite well in depicting areas that will become convectively unstable or stable. In this paper, however, we hypothesize that an alternative formulation in isentropic coordinates will further improve predictions of the movement of moisture features observed by the GOES sounder. Since the retrievals are made from the clear sky where diabatic processes are at a minimum, the flow in the atmosphere can be assumed to be adiabatic, i.e. the flow is not along isobaric surfaces, but is instead along isentropic (constant potential temperature) surfaces. Not only does the isentropic framework more accurately represent the flow of these particular observations in the atmosphere, but it also depicts adiabatic lift and can retain information in the observations about total isentropic layer mass and moisture. Given the isobaric version of the NearCast model works well in improving forecasts of the timing and location of convection, and the assumption that flow of the observations at hand is adiabatic, this study seeks to understand the full advantage of the extra information and increased accuracy added by running the model in an isentropic framework.

First, a detailed literature review will be presented which will highlight the research breakthroughs leading up to and influencing this work. Next, the data used in the

model and how it is obtained will be presented, followed by a description of the model configuration. In the main results section, a very thorough case study will be presented, followed by several brief, supplementary case studies. Finally, the study will be summarized and possibilities for future related work will be highlighted.

2 Background

2.1 Early History of the Isentropic Vertical Coordinate

In this section, the history of vertical coordinate systems used in the atmospheric sciences will be discussed, with particular attention paid to that of isentropic coordinates. The history of weather analysis in isentropic coordinates will then be tied in with that of Lagrangian trajectory models, of which the NearCast model is one. Advantages and disadvantages of isentropic analysis will finally be outlined.

The discussion of which vertical coordinate system would be best for weather analysis began in the 1930s (Bleck, 1973). This came as a result of synoptic upper air observations becoming substantially more numerous with the development of the radiosonde. Scientists had enough data to make weather analysis charts at multiple vertical levels of the atmosphere, leading them to ask the question: On what vertical coordinate should we view the evolution of the atmosphere? Early on, Germany and much of Europe chose pressure as their vertical coordinate, while the weather services of the United States and Great Britain initially drew their charts on constant height levels.

Shaw (1933) was one of the first to advocate for isentropic analysis. He developed a

method for plotting upper air data on constant entropy charts (iso-entropy), on which potential temperature is conserved. Shaw proved that the state of the atmosphere could be simplified using this method as opposed to plotting on constant height levels. A case study over Europe performed by Shaw showed that where air flowed upward along the constant entropy surface, precipitation was observed. Shaw also noted some of the disadvantages of isentropic charts, including isentrope-land intersection and the fact that diabatic processes can disrupt the continuity of isentropic flow.

Some of the early proponents of isentropic analysis following Shaw included Rossby and Namias. Rossby (1937a) argued that isentropic charts represent the true motion of air in the atmosphere much more accurately than constant height charts. He noted that when using constant height charts, air masses can appear and disappear between two consecutive charts as the result of vertical displacements, while on isentropic charts, flow is continuous. He also outlined some of the main advantages of isentropic analysis over other frameworks. Namias (1939) discussed how plotting temperature and moisture on constant height charts only made the vertical structure of atmospheric disturbances appear more complicated than they really were. Such favorable arguments helped lead the United States Weather Bureau in the late 1930s to start transmitting data important for isentropic analysis over the weather teletype network (Bleck, 1973). The research of several others would also involve the use of isentropic analysis in the early 1940s (Montgomery, 1937; Byers, 1938; Spilhaus, 1940; Starr, 1940; Neamtan, 1944).

By the mid-1940s, however, the United States weather bureau stopped transmitting isentropic data due to a lack of widespread interest in this method of analysis (Bleck,

1973). At the same time, constant height maps were pretty much abandoned as well, with isobaric coordinates becoming the most commonly used vertical coordinate system around the world, operationally and in the research community. There were several key reasons that are attributed to the relative disuse of isentropic analysis and rise of the isobaric coordinate system in the early 1940s:

1. Construction of isentropic charts was time-consuming in the pre-computer age (data was measured at constant pressure levels, and had to be interpolated to constant potential temperature levels). This made it difficult for the charts to be available in a timeframe suitable for an operational environment (Moore, 1987).
2. The Montgomery stream function ($M = \Phi + c_p T$ where, $\Phi = gZ_\theta$, g is the acceleration of gravity, Z the height of the isentropic surface, c_p the specific heat of air at constant pressure, and T the temperature in Kelvin) formulated by Montgomery (1937), which defines geostrophic flow on isentropic surfaces, was being computed incorrectly. This was causing the geostrophic wind law in isentropic coordinates to not work (Bleck, 1973).
3. With World War II came the rise of the aviation industry. Since aircrafts were flying at constant pressures, there was a practical need to have weather data (especially winds) plotted on constant pressure surfaces (Moore, 1987).
4. The success of the Pettersen-Sutcliffe development equation, which related vorticity advection at 500 hPa to surface cyclonic development, required the use of isobaric charts (Pettersen, 1956).

Analysis in isentropic coordinates was pretty rare from the early 1940s through the late 1950s (especially in the operational community) before Danielsen (1959) discovered and fixed the flaw in the calculation of Montgomery stream function. Essentially, the issue was that the two terms in Montgomery stream function were being calculated separately, when they are actually related through Poisson's equations in isentropic coordinates. It was found that computing the two terms independently led to errors as high as 20% in their sum (Wilson, 1985). This discovery and solution by Danielsen was really what led to the resurgence of isentropic analysis, at first in diagnostic studies, and later in atmospheric models (Moore, 1987).

2.2 Atmospheric Trajectories

The resurgence of isentropic analysis corresponded with the rise of a new diagnostic tool: atmospheric trajectories. Danielsen (1961) outlined the first widely used (implicit) method for computing parcel trajectories. Through several experiments, he showed that isobaric trajectories can differ drastically from isentropic trajectories (horizontally and vertically), especially in situations with vertical motions and gradients in vertical motions. The isentropic trajectories matched the flow of actual air way more accurately than isobaric trajectories, primarily because the horizontal component of flow implicitly includes the vertical component, providing a simple way to represent the three-dimensional flow of air. Using the isentropic framework eliminates the errors introduced when calculating vertical motions separately as is the case in the isobaric framework. Danielsen's method for computing trajectories on isentropic surfaces in-

volves simultaneously solving the following kinetic energy and displacement equations:

$$M_2 - M_1 + \frac{1}{2}(V_2^2 - V_1^2) = \frac{\Delta M_1 + 2\Delta M_m + \Delta M_2}{4} \quad (1)$$

$$D = \frac{V_1 + V_2}{2} \Delta t \quad (2)$$

where M_1 and M_2 are the initial and final mass fields (height in pressure coordinates, Montgomery stream function in isentropic coordinates), V_1 and V_2 are the initial and final velocity fields, subscript m represents the midpoint between times 1 (initial) and 2 (final), and Δt is the time step.

Danielsen's trajectory work marked the initial use of three-dimensional trajectories as a tool for diagnosing atmospheric transport and exchange processes. Some early diagnostic research in which isentropic trajectories proved to be useful included: stratospheric-tropospheric air mass exchange (Danielsen, 1968; Reiter, 1972), three-dimensional moisture structure and transport (Danielsen, 1966, 1967; Buzzi & Rizzi, 1975), the dispersal of upper atmospheric pollutants and nuclear contaminants (Reiter, 1972) and the kinetic energy budget for extra-tropical cyclones (Sechrist & Dutton, 1970).

Danielsen (1964) conducted a significant study which utilized the implicit trajectory approach to diagnose the potential stratospheric-tropospheric exchange of nuclear contaminants. Isentropic trajectories showed that air from the stratosphere was being transported downward into the troposphere. Aircraft measurements of nuclear contaminants confirmed that there was indeed an exchange between the two atmospheric layers.

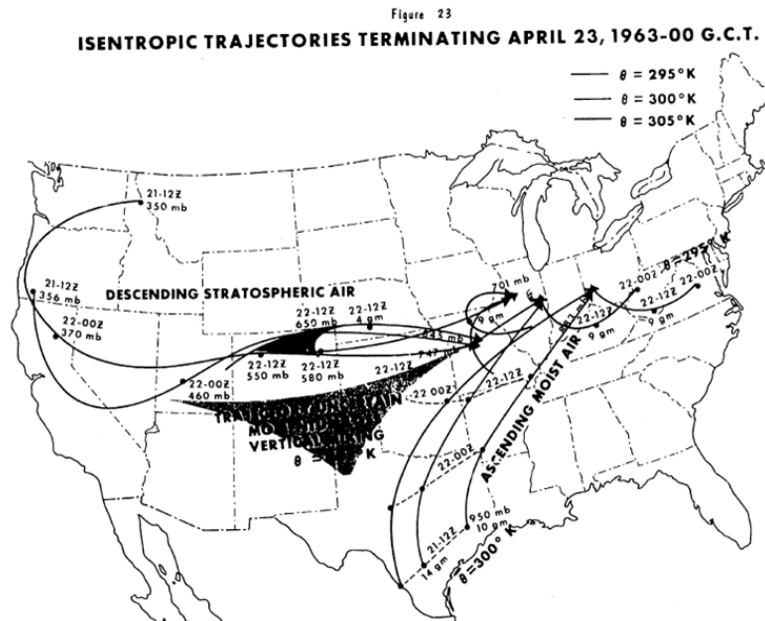


Figure 2: Back trajectories computed along the 295, 300, and 305 K isentropic surfaces in the vicinity of the April 23, 1963 tornado outbreak. Analysis in text. From Danielsen (1964).

During the period of the experiment, there was a significant tornado outbreak in Illinois. Back trajectories confirmed that the upper-level dry air observed encroaching into the area of the tornado outbreak had originated from the stratosphere and descended into the upper troposphere from the west (Fig. 2). At the same time, warm moist air had ascended from the south into the area. The strongest convection developed along the leading edge of the upper-level dry air as it overlaid the low-level moisture. Trajectories showed this important atmospheric phenomenon long before satellite water vapor observations revealed the same relationship. Danielsen's diagnostic study proved that three-dimensional, adiabatic transport is an important atmospheric process, and can be successfully depicted using isentropic trajectories.

Despite its success in diagnosing atmospheric transport, Danielsen's implicit ap-

proach does have some drawbacks. For one, the simultaneous solution of (1) and (2) often leads to more than one unique solution for anticyclonic trajectories (Danielsen, 1961). Also, the large time step and implicit nature of the scheme make it difficult to account for variable parcel accelerations that occur along the trajectory path (Petersen & Uccellini, 1979).

Such drawbacks led Petersen & Uccellini (1979) to develop an explicit method for computing atmospheric trajectories on isentropic surfaces. This technique, designed for a Lagrangian system and based on the discrete formulation of Greenspan (1972, 1973), takes into account local mass field tendencies and resulting variable parcel accelerations occurring along the parcels entire path. It has proven to be a rapid and economical way of computing trajectories, is stable in the presence of geostrophic departures and local mass field tendencies, and produces results that match well with observations. More details about this method will be given when the model configuration is described in section 4.

Kocin *et al.* (1986) utilized the explicit approach for computing parcel trajectories while diagnosing the 1979 Red River Valley tornado outbreak. In this diagnostic study, trajectories of moisture observations were computed along a low-level isentropic surface in the vicinity of the outbreak. The moisture data came from the SESAME experiment, a network of 3-hourly balloon observations across the south-central United States. Results showed moist air ascending and accelerating into the region from the south, while dry air was intruding from the southwest. The trajectories not only related the transport of moisture into the area of the storms with the development of the low-level jet,

but also depicted the eastward movement of the dry line and the convergence of the two contrasting air masses. This study was significant in proving that Lagrangian trajectories need not be limited to just diagnostic studies, but also had potential for use in a forecast setting.

The Kocin *et al.* (1986) study was a seed for expanding the use of trajectories from diagnostic studies to use as a forecasting tool as well, leading to the initial development of the NearCast model in the late 2000s. The NearCast model, a Lagrangian trajectory model, utilizes the explicit scheme developed by Petersen & Uccellini (1979) to compute trajectories for GOES sounder temperature and moisture observations. Originally written for an isobaric framework, this paper introduces a new version of the model that computes parcel trajectories along constant isentropic surfaces.

2.3 Isentropic Coordinates in NWP

During the same period (1970s through the 1990s), the advantages of isentropic coordinates were being considered in Eulerian NWP models. The first successful attempt at this was done by Eliassen & Raustein (1968). Because of issues in the boundary layer (isentropic-surface intersection, super-adiabatic layers, and non-adiabatic flow) however, pure isentropic coordinate models are not too desirable. This led to the development of a hybrid sigma-isentropic coordinate scheme outlined in Bleck (1978a,b). This type of model uses the terrain-following sigma coordinate in the lowest part of the model while still taking advantage of isentropic coordinates in the free atmosphere.

One of the most notable hybrid models was the Rapid Update Cycle (RUC) model

which went into operation as part of the National Meteorological Center's (NMC, now part of NCEP) operational analysis/forecast system (Benjamin & K. J. Brundage, 1994). The RUC model was a version of the Mesoscale Analysis and Prediction System (MAPS), an analysis/forecast data assimilation system developed to take advantage of the increase in asynoptic meteorological observations. The model was operational from 1994 into 2012, and was a short-range forecasting tool. Information on the hybrid-b coordinate system used in the RUC model, which was originally used in an ocean model (Bleck & Boudra, 1981), can be found in (Bleck & Benjamin, 1993).

2.4 Advantages of Isentropic Analysis

The advantages of the isentropic vertical coordinate system have been outlined extensively in Bleck (1973), Uccellini (1976), and Moore (1987), and are summarized here.

1. In the free atmosphere, isentropic surfaces act as material surfaces over synoptic time scales. Diabatic processes are the only significant processes that act to penetrate these surfaces, such as the release of latent heat in rising, saturated air and the addition of sensible heat in the planetary boundary layer (PBL) (Rossby, 1937b).
2. Since isentropic surfaces vary with pressure and height, the horizontal component of flow along an isentropic surface implicitly includes the adiabatic component of vertical motion as well. This removes the need to calculate vertical motion

separately, as is the case in other coordinate systems (Danielsen, 1961).

3. Moisture transport on an isentropic surface is three-dimensional, with the vertical advection of moisture included in the horizontal part. The vertical movement of moisture has often been ignored in other coordinate systems, leading to discontinuities and a lack of coherency in the moisture fields (Oliver & Oliver, 1951).
4. Isentropic surfaces run parallel to fronts, making variables appear continuous in the vicinity of frontal zones. Pressure surfaces cut through fronts, causing fields across them to look discontinuous with sharp gradients. Isentropic surfaces show the terrain-like, three-dimensional nature of flow in the atmosphere, especially around frontal zones (Rossby, 1937b).
5. Static stability can be determined from the separation of isentropic surfaces (Moore, 1987). Similarly, the total amount of mass in an isentropic layer can be determined from the separation of consecutive levels, or inverse static stability. This can be used to determine the total amount of moisture in an isentropic layer. Such information is useful in determining the potential for heavy precipitation.

2.5 Shortcomings of Isentropic Analysis

Despite the many advantages of using isentropic coordinates as the vertical coordinate, it does have its drawbacks, many of which are described by Moore (1987) and summarized here:

1. Isentropic surfaces may intersect the ground, often at steep angles. This causes analysis near the ground to be suspect.
2. Diabatic processes disrupt the continuity of flow along an isentropic surface, causing motion through a surface.
3. In super-adiabatic layers, an isentropic surface may repeat itself. A vertical coordinate should change monotonically with height.
4. Different isentropic surfaces must be chosen for analysis based on the season, since potential temperature is constantly changing height.
5. Though the sigma-isentropic hybrid model resolves some of these drawbacks, it introduces new problems. NWP, and more specifically data assimilation, becomes extremely complicated along the interface of two coordinate systems. Error is introduced into the model, and run times become long.

3 Data

3.1 Temperature and Moisture Observations

For complete details into the GOES sounding retrieval process, see Li *et al.* (2008). Only a brief conceptual summary of the process is discussed in this section.

The temperature and moisture profile data used in the NearCast model and discussed in this paper come from the GOES 13 (GOES-East) sounding device, introduced

in section 1. The satellite measures radiation (or radiances) emitted from Earth at each of the 18 IR channels, or range of wavelengths. Gases at different levels in the atmosphere absorb and emit radiation to various degrees as a function of the wavelength that is being sensed. The spectral channels used are chosen strategically based on the locations of known absorption regions and windows in the IR spectrum. Radiances measured within carbon dioxide and water vapor absorption regions and window regions are, together, used to produce vertical profiles of temperature and moisture, the process of which is described in this section.

An atmospheric absorption region is a range of wavelengths in which a particular gas absorbs and emits radiation. At the center of an absorption region, attenuation of upwelling radiation is strongest, causing the atmosphere to appear opaque from space. The brightness temperatures are coldest here because radiation is being emitted from high in the atmosphere. At wavelengths away from the center of an absorption region, or at the ‘wings’, attenuation by the gas is weaker, causing the atmosphere to appear more transparent from space. Brightness temperatures are warmer because radiation is being sensed from closer to the warm Earth surface. A window region is a range of wavelengths where radiation is not attenuated by a gas, allowing a satellite to measure radiances from close to Earth’s surface. By sensing radiation at differing wavelengths between the wing and the center of an absorption region, the radiances can be used to represent successively higher layers of the atmosphere.

The approximate layer in the atmosphere from which the radiance information emanates is determined by the weighting function for each wavelength. The weighting

function, which is the derivative of the transmittance with respect to height, represents the approximate contribution of each layer in the atmosphere to the total radiation being emitted to space at the wavelength. It peaks in the layer of the atmosphere that contributes the most radiation.

The GOES temperature and moisture soundings used by the NearCast model in this study are produced using a physical retrieval algorithm that simultaneously solves for the surface skin temperature, atmospheric temperature, and atmospheric moisture from the radiance measurements. A first guess profile from an NWP model is utilized to begin the retrieval process. The radiances calculated from this model profile are adjusted, along with the profile itself, until the calculated radiances match the radiances measured by the satellite. Once the radiances match, the adjusted profile is the retrieved profile. Temperature profiles are produced at 40 pressure levels from 1000 to 0.1 hPa, while the moisture profiles are at the same levels up to 300 hPa. These “levels” actually represent layer averages of the atmospheric constituent since the radiances measured by the satellite are the results of emission from broad layers. The ability to view moisture in the lower layers increases with drier upper-level air as the atmosphere above the moisture is more transparent. CIMSS processes its own retrievals, which are used in the NearCast model. For the isentropic version of the model, a linear interpolation is applied to these soundings so that temperature and moisture data are available on potential temperature levels every 2 K.

In the isobaric NearCast model, the lower level is chosen to be 780 hPa, which represents an average across an approximate 700-900 hPa layer. This layer is low enough

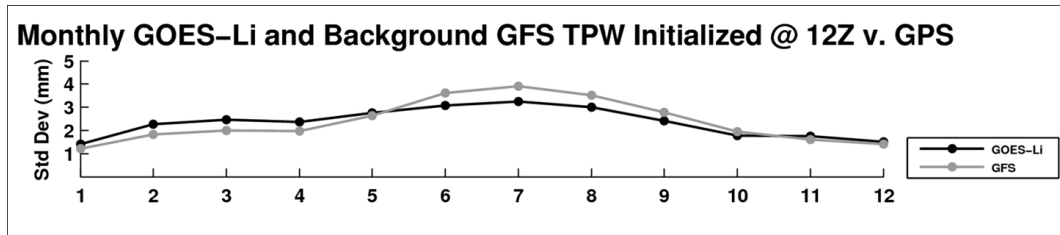


Figure 3: 2011 monthly comparisons of Global Positioning System (GPS) total precipitable water (TPW) measurements with GOES TPW (Li retrievals) and GFS first guess TPW. Standard deviations (Std Dev) were calculated wherever there was a collocation of a GPS site and a GOES retrieval. Analysis in text. From Petersen *et al.* (2012).

in the atmosphere to capture information about low-level moisture, but high enough so that the high land surface emissivity does not negatively impact the observations, and friction is negligible. At this layer, the model can effectively predict the movement of low-level moisture in the atmosphere. The upper-level is chosen to be 500 hPa, representing approximately a 400-600 hPa layer, where the presence of upper-level dry air is observed well by GOES. These layers correspond to the levels of the maximum weighting functions for the 7.4 and 7.0 μm channels on the sounder. In the isentropic NearCast model, the upper and lower levels are adjusted to vary with season and correspond roughly with these same levels.

The quality of the GOES moisture retrieval data is represented in Fig. 3. It is apparent that the information observed by the GOES sounder is an improvement upon the GFS model first guess in the warm season, when NWP short-term precipitation forecast skill was shown to be the poorest.

3.2 Wind and Mass Field Data

Predicted wind and geopotential fields are required to compute the evolution of the parcel trajectories. For this study, these data were obtained from the GFS model on a .5 degree grid at 50 hPa intervals in the vertical. For the isentropic NearCast model, a linear interpolation is applied to move the data to isentropic coordinates at 2 K intervals using the General Meteorological Package (GEMPAK). The isentropic fields derived from the GFS data include winds, Montgomery stream function as the mass field (as opposed to height in pressure coordinates) and pressure, all on isentropic levels. Observations that have trajectories underground are not included in the model output.

4 Methods

The NearCast model uses the explicit method for computing trajectories developed by Petersen & Uccellini (1979) and summarized here. This approach works in a Lagrangian framework and computes trajectories dynamically (uses both mass and velocity fields). The main difference between the approach outlined by Petersen & Uccellini (1979) and that used in the NearCast model is that the latter uses forecast gridded fields, while the former uses analysis fields for computing trajectories. The NearCast model requires a gridded wind field at the initial time step, with mass fields at every other time step to accelerate the parcels. The parcels for which the trajectories are computed are the temperature and moisture retrieval data discussed in the previous section. The details about how the NearCast model works is discussed in this section.

The necessary information for running the model includes the gridded fields and the observation data as well as a grid projection file and a model configuration file. The grid projection file holds information about the NearCast model grid geometry. The configuration file includes input file names, observation variables to be used, model time step, output time step, interval between gridded data, and the level on which the trajectories are to be computed.

First, the gridded wind and mass fields are read in and interpolated to a selected model grid. Layer-averaged winds (representative of the depth of the GOES observations) are then calculated for the initial time for the level on which the trajectories are to be computed. Mass field gradients are also computed at the initial time across the grid for use in the acceleration equations. The initial wind and mass field gradients are then assigned to every GOES sounding location and trajectory level using a bi-quadratic interpolation technique.

The trajectory calculations for each observation are made as follows. First (at every time step), the acceleration, a , of each parcel is computed using the inviscid equations of motion,

$$a_x^t = -\frac{\Delta M^t}{\Delta x} + f^t v^t \quad (3)$$

$$a_y^t = -\frac{\Delta M^t}{\Delta y} - f^t u^t \quad (4)$$

where u and v are the velocity components in the x and y directions, respectively, M is the mass field, f is the coriolis parameter, and t is the current time step. M represents the geopotential field in isobaric coordinates and the Montgomery stream function field

in isentropic coordinates. The acceleration of each parcel is the result of a combination of the pressure gradient force and the coriolis force. Note the absence of the highly non-linear advective terms, thus avoiding a source of error that requires extremely small time steps in Eulerian models.

For the initial time step only, a special startup formula is used to calculate the parcels u and v velocity components

$$u^1 = u^0 + a_x^0 \Delta t \quad (5)$$

$$v^1 = v^0 + a_y^0 \Delta t \quad (6)$$

where t is the time step. At every subsequent time increment, the new u and v velocity components are calculated using Greenspan's discrete formulation,

$$u^{t+1} = u^t + \Delta t \left(\frac{3}{2} a_x^t - \frac{1}{2} a_x^{t-1} \right) \quad (7)$$

$$v^{t+1} = v^t + \Delta t \left(\frac{3}{2} a_y^t - \frac{1}{2} a_y^{t-1} \right) \quad (8)$$

Finally, the computation of each parcels new x/y location on the grid can be made:

$$x^{t+1} = x^t + \frac{1}{2} \Delta t (u^{t+1} + u^t) \quad (9)$$

$$y^{t+1} = y^t + \frac{1}{2} \Delta t (v^{t+1} + v^t) \quad (10)$$

Mass field gradients are then bi-linearly interpolated in both time and space to the new parcel locations for use in calculating the next parcel accelerations. In these finite difference equations, superscript t represents the current time, while t+1 and t-1 represent the next and previous time steps, respectively.

Equations 5 and 6 are necessary since there is no previous acceleration available at the initial time step like that seen in equations 7 and 8. The time step used in the NearCast model is 10 minutes, with parcel location information saved at every three time steps (30 minutes). The half-hourly parcel data are saved from 10 successive cycles so that they can be used to enhance output of future model runs. It should be noted that although inertial error growth in the trajectories due to initial wind inaccuracies becomes greatest about five to six hours into the forecast, the accumulated errors remain small through 10 hours. The NearCast model updates every hour as new GOES observations become available.

Once all trajectories have been calculated using the most recent GOES observations, the irregularly spaced trajectory information from the current run is combined with information from 10 previous cycles to produce a sequence of output products at half-hourly intervals for display and distribution in grib2 format. Typically, the output grid spacing is chosen to be approximately equal to that of the original GOES observations. Because the GOES sounder cannot make observations in areas considered to be cloud covered, there are often gaps in displays of only the observed data. The inclusion of older trajectories from previous NearCast model cycles in current analysis and forecast products helps to fill the data void areas, greatly increasing data coverage in the final products. The technique used to integrate current observations with previous trajectories onto regularly-spaced output grids needed to generate graphical displays proceeds as follows, and is shown graphically in Fig. 4.

For analysis displays, starting with the oldest forecast trajectories (initiated 10 hours

		Forecast Valid (UTC)																					
		0000	0100	0200	0300	0400	0500	0600	0700	0800	0900	1000	1100	1200	1300	1400	1500	1600	1700	1800	1900	2000	
Forecast Initialization (UTC)	0000	A	1	2	3	4	5	6	7	8	9	10											
	0100		A	1	2	3	4	5	6	7	8	9	10										
	0200			A	1	2	3	4	5	6	7	8	9	10									
	0300				A	1	2	3	4	5	6	7	8	9	10								
	0400					A	1	2	3	4	5	6	7	8	9	10							
	0500						A	1	2	3	4	5	6	7	8	9	10						
	0600							A	1	2	3	4	5	6	7	8	9	10					
	0700								A	1	2	3	4	5	6	7	8	9	10				
	0800									A	1	2	3	4	5	6	7	8	9	10			
	0900										A	1	2	3	4	5	6	7	8	9	10		
	1000											A	1	2	3	4	5	6	7	8	9	10	

Figure 4: Graphical depiction of how the NearCast model uses up to 10 hours of old observations from previous model forecasts in its current analysis and forecast display products to fill in data void area. Output from every forecast hour in the column above a given analysis or forecast hour is used in that analysis or forecast display. Detailed explanation of this process in text.

earlier), the average of all parcels that are predicted to be located within a very small radius of each output grid point is calculated. This provides a first guess field in all geographical areas where trajectories were available. This process is repeated successively using trajectories from previous nine through one hour forecasts which are valid at the analysis time. Averages are again calculated for each grid point and corrections are applied to the first guess field. If no first guess is available, the grid point is populated directly using the most recent trajectory data. As the forecast time decreases, so does the averaging radius. Finally, the current set of GOES observations are included and given the most weight. This process produces an image which preserves all current GOES observations in full detail, yet provides information projected from previous GOES observations to fill ‘data gaps’ that occur in the IR data sets after clouds form or move over an area.

For the forecast displays, grids are produced using a similar procedure at 30 minute intervals out to nine hours. For example, to produce the one hour forecast output grids, 10 hour trajectory data from the run initialized nine hours earlier are used first to create the first guess field. Then, nine hour forecast data from the trajectories generated eight hours earlier, eight hour data from the trajectories generated seven hours earlier, etc., through one hour projections of the current observations are used to make successive corrections to the first guess field or provide new information to grid points. Again, the most recent data are given the largest influence.

5 Results

Several case studies will be presented to show the NearCast model's ability to depict and predict areas with the highest (and lowest) potential for convective activity. The goal is to identify regions where dry air will override moist air in the near future. The first case study will be described in detail, including the use of both the isobaric and isentropic versions of the model while introducing the parameters used in each and explaining how to interpret the model output. Three other, supplementary case studies will then be discussed in much less detail using the isentropic version of the model only. For each case study, a brief description will first be given for the event, followed by an analysis of the NearCast model output, including how the data is properly interpreted.

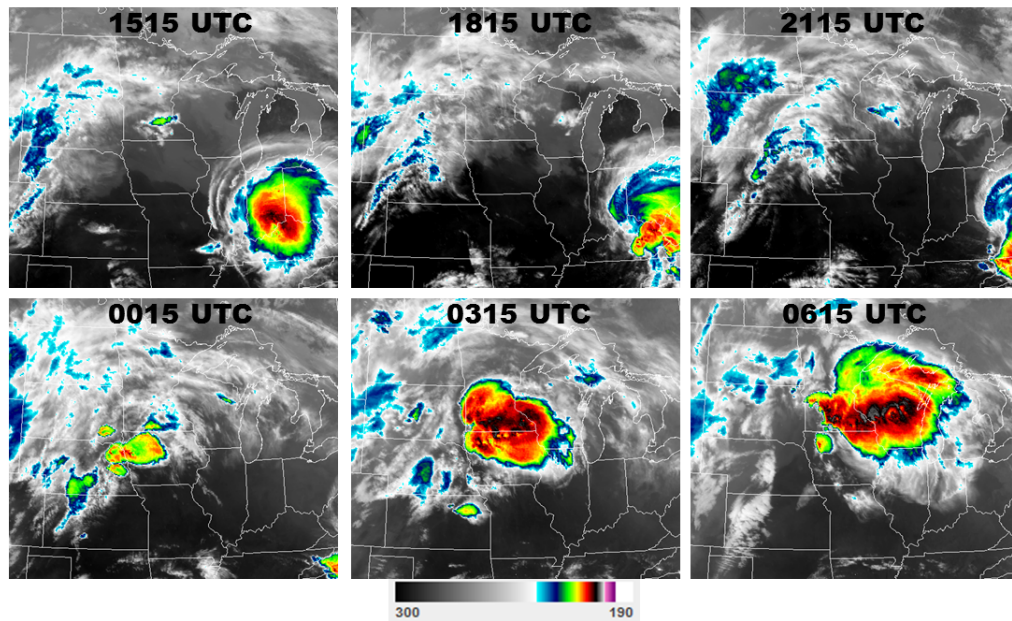


Figure 5: 3-hourly sequence of $10.7 \mu\text{m}$ imagery measured by the GOES-East imager on April 09-10 2011.

5.1 April 09, 2011-Isobaric NearCast

The first case occurred from the evening of April 09, 2011 into the early morning hours of the next day. Deep convection began its initial development in far east-central Nebraska between 2200 and 2300 UTC moving east-northeast (Fig. 5). The severe convection and associated thunderstorm quickly spawned a strong EF3 tornado as it moved into northwest Iowa, though it never produced widespread, heavy rainfall (Fig. 6, inset). The 3/4 mile wide tornado damaged or destroyed 50-60% of the town of Mapleton, Iowa (Staff, 2011). The tornadic cell, also producing large hail and damaging winds along its path, traveled northeast into north-central Iowa by 0400 UTC (Fig 6). Afterwards, this initial area of convection and associated severe thunderstorm weakened considerably as evidenced by the SPC reports and satellite imagery.

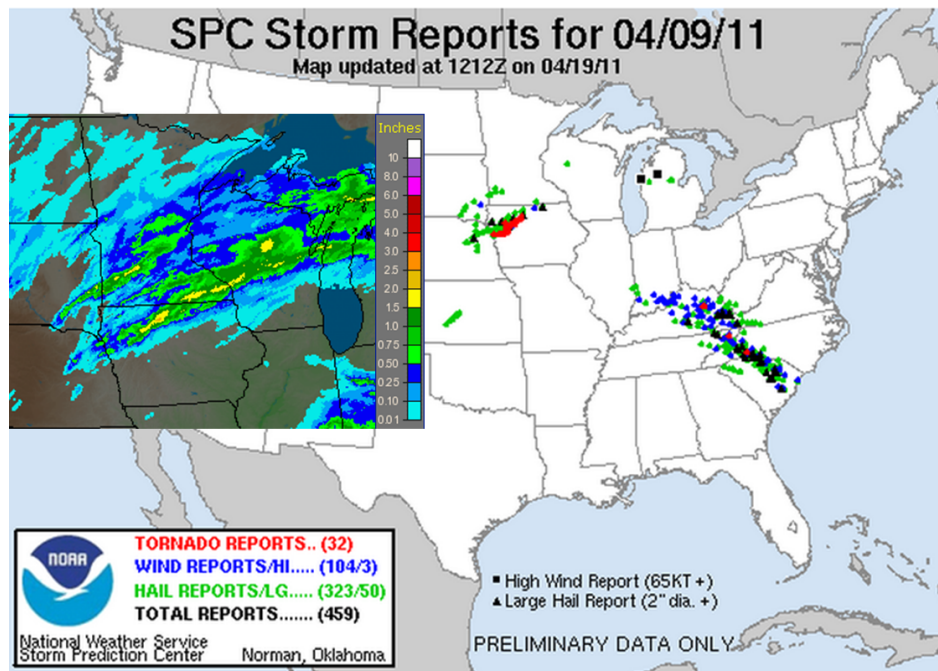


Figure 6: Storm Prediction Center (SPC) severe storm reports for April 09, 2011 (the 24 hour period ending 1200 UTC on April 10, 2011). Inset is observed precipitation for the same period, obtained from the National Weather Service (NWS) Advanced Hydrologic Prediction Service.

Between 0200 and 0400 UTC, a new area of less severe but more widespread and longer-lasting convection developed in southeast Minnesota, ahead of the weakening earlier convection. These new storms produced much heavier and widespread rainfall as they tracked across southeast Minnesota into central Wisconsin by the early morning hours of the 10th (Fig. 6, inset).

The performance of the isobaric version of the NearCast model over the duration of this event will be discussed first. As previously mentioned, the ultimate goal of the NearCast model is to improve short-term forecasts of stability and instability by predicting where dry air will move over moist air. Instability is a necessary ingredient for convection to occur, while a stable atmosphere will inhibit convection. Areas that

experience the most rapid destabilization tendencies in the model typically have the greatest potential for convective development.

One way of gauging the stability of the atmosphere is to look at the convective instability, a layer instability. Assume there is a deep atmospheric layer (780 to 500 hPa is used in the NearCast model) with warm, moist air below relatively cool, dry air. If some dynamical forcing causes the entire layer to be lifted, the bottom of the layer will reach its Lifted Condensation Level (LCL) much quicker than the top. This will cause the air at the bottom of the layer to become saturated, leading to latent heat release (LHR), warming this part of the layer. As the whole layer continues to rise it will cool adiabatically, but the bottom of the layer will cool much more slowly than the top due to the LHR. The disproportional cooling causes the layer to eventually become absolutely unstable. The greater the discrepancy of temperature and moisture between the top and bottom of the layer, the more unstable the atmosphere may become, increasing the potential for and strength of convection. In a practical sense, convective instability is present when a dry, cool upper-level airmass overlays warmer and more moist air below. As mentioned earlier, convection tends to form along the leading edge of upper-level dry air as seen on satellite water vapor imagery.

The lapse rate in equivalent potential temperature (θ_e) is used to gauge the convective stability of the atmosphere as follows:

$$\frac{\partial\theta_e}{\partial z} > 0, \text{ convectively stable} \quad (11)$$

$$\frac{\partial\theta_e}{\partial z} < 0, \text{ convectively unstable} \quad (12)$$

θ_e includes information about the temperature and moisture content of the air. Its computation, and that used in this paper, can be found in Bolton (1980). θ_e is a measure of the total thermal energy of a parcel of air and accounts for both the adiabatic temperature change a parcel undergoes when it is lifted or lowered in the atmosphere and the temperature change due to latent heat release. This makes the variable quite useful in comparing the temperature and moisture content of different levels of the atmosphere, as is the case when used to determine convective instability. For example, if a warm moist air mass (high θ_e air) at the lower levels moves below a much cooler and drier airmass (low θ_e air), that location is or is becoming convectively unstable. Given the proper forcing, such a location could destabilize and be ripe for convective development.

In the NearCast model, deep layer convective stability is determined by computing the difference between θ_e at the upper and lower level ($\theta_e^{500hPa} - \theta_e^{780hPa}$). The vertical θ_e difference, or lapse rate, reveals whether the atmosphere is convectively stable or unstable, as well as the degree of stability. When the θ_e difference is negative (positive), θ_e is decreasing (increasing) with height through the layer, so the atmosphere is convectively unstable (stable). Tendencies in θ_e difference over the nine hour period are also important in that they reveal which areas will destabilize the quickest and are, therefore, even more likely for convective development. The deep-layer θ_e difference parameter is an objective way to portray the temperature and moisture information from the GOES sounder and to mimic what is observed in water vapor imagery. It should be noted that many other processes can be involved in actually defining the kinds of

instability that occur with different events throughout the year in different geographic locations.

As mentioned, the parcels for which trajectories are computed include the temperature and moisture satellite retrievals from the GOES sounder. The temperature and moisture data, along with the pressure level of the retrieval, are used to compute θ_e at two sounding levels. This information is used to determine the convective instability of the layer at the time of the observations based on the θ_e lapse rate. The trajectory model extends the utility of the observations by projecting them into the future.

The 1500 UTC NearCast cycle for the April 09, 2011 case is discussed first, initialized approximately 7.5 hours before the onset of convection in eastern Nebraska. Initial attention is focused on the evolution of low-level (780 hPa) θ_e over the nine hour forecast since locally high values of lower tropospheric θ_e are an essential component for most strong convection (Fig. 7). There was fairly strong southerly to southwesterly flow forecasted from Texas north into southern Minnesota throughout the period drawing up warm, moist (high θ_e) air from the south. At the analysis time, the plume of relatively high θ_e air stretched from southern Texas into Kansas with a θ_e maximum located in central Kansas. θ_e just to the north and east of the local maximum was considerably lower. By the end of the NearCast cycle at the 9 hour forecast (valid at 0000 UTC shortly after convection began to develop in eastern Nebraska) the trajectory model had moved the maximum through Kansas and eastern Nebraska into northwest Iowa. The rapid moistening and warming in the domain at the lower level was the first clue that convective development was possible.

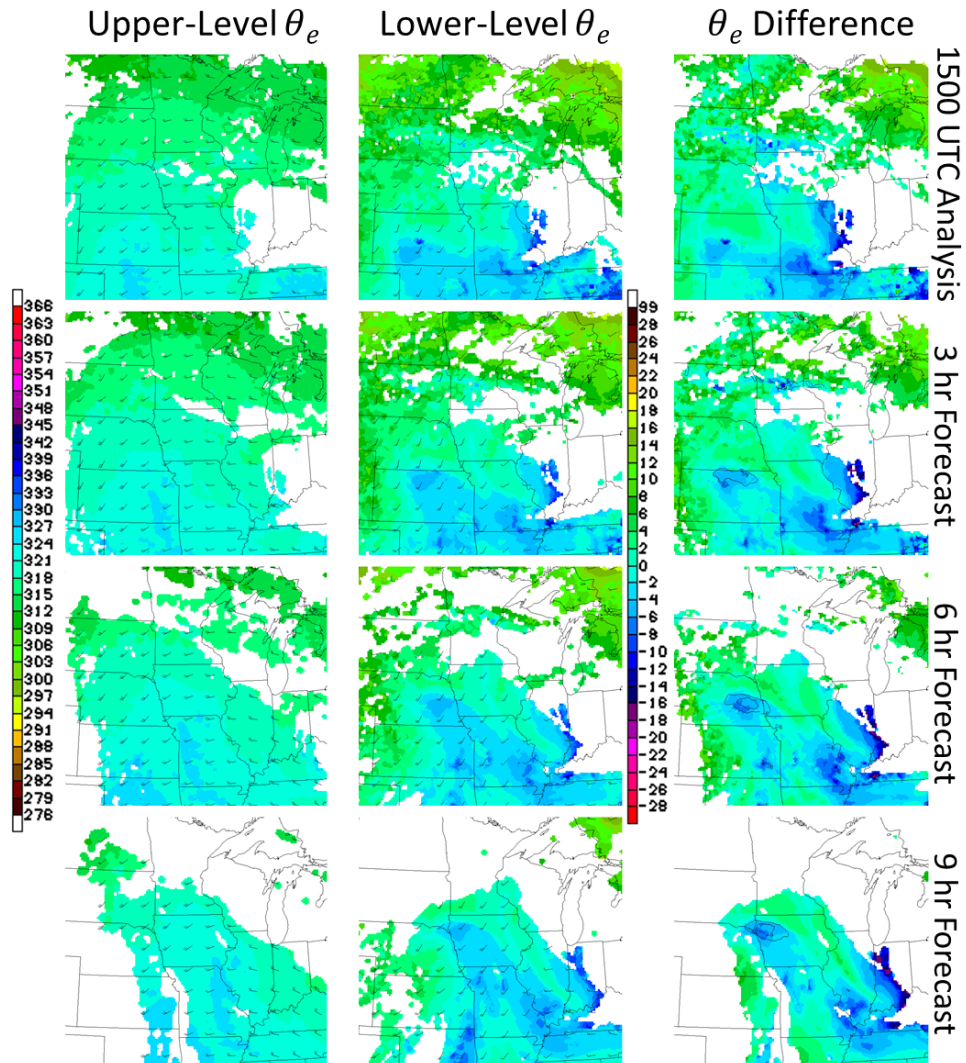


Figure 7: 1500 UTC April 09, 2011 isobaric NearCast model cycle. Analysis and forecast displays use the most recent (1500 UTC) observations from the GOES sounder, as well as previous model cycle trajectories from as far back as 0500 UTC. Upper level is 500 hPa, lower level is 780 hPa, and θ_e difference is upper-level minus lower-level θ_e . Colorbar on left represents θ_e . Higher (lower) values indicate warm and moist (dry and cool) air. Colorbar on right is θ_e difference. Negative (positive) values indicate the layer is convectively unstable (stable). Winds are in knots. White areas are where no retrievals were made (or projected into) due to the presence of cloud cover. Black contours in θ_e difference plots are θ_e difference 2 hour time tendencies, starting at $-6\text{K}/2\text{ hr}$, decreasing by 3 K increments. More contours (more negative values) signify more rapid destabilization.

In the mid troposphere (500 hPa), θ_e values were considerably lower throughout the region, indicating the air was drier and cooler than below (Fig. 7). Flow at this level was forecasted to have more of a westerly component during the period with relatively dry air moving into eastern Nebraska by 2100 UTC.

The vertical wind shear (speed and directional) is another important ingredient in the development and maintenance of severe weather, and can be analyzed and predicted by comparing the winds at the two levels in the NearCast model. Veering winds with height indicate favorable directional shear for severe weather, while increasing wind speed with height indicates favorable speed shear. With this case, both types of shear were predicted to increase in eastern Nebraska throughout the 1500 UTC NearCast cycle.

Figure 7 also shows the evolution of the θ_e difference parameter throughout the 1500 UTC NearCast cycle. Initially, there was a local maximum of strong convective instability in central Kansas with stable air lying just ahead of it to the northeast. Moving forward in the forecast cycle, the ridge of instability was forecasted to advance north-northeast into eastern Nebraska and finally into northwest Iowa by 0000 UTC. This is precisely the location where and time when convection that spawned the strong tornado developed. The instability was a result of the westerly upper-level dry air overlaying the northeast-bound low-level moisture. Comparing Fig. 5 with Fig. 7, the location of strongest convection at 0000 UTC lied within the forecasted instability maximum.

It is important to note that, not only was there an area of strong instability fore-

casted to move through the region, but also that the air ahead of the instability maximum was quite stable. This setup meant that locations along a not so wide path from central Kansas to northwest Iowa would see a rapid destabilization over the nine hour period. In the area of tornadic development, the atmosphere was actually becoming more stable before rapidly destabilizing, capping the energy that had been building up during the day. In other words, because the atmosphere was initially convectively stable, thermal energy building up in the lower atmosphere due to daytime heating was trapped, and would likely not be released until the area became convectively unstable. The most rapid destabilization (negative θ_e difference time tendencies) is also highlighted in Fig. 7, helping to narrow down the regions of instability that were most likely to experience convection. Maximum destabilization tendencies of -9 K/2 hr were forecasted in northwest Iowa by 0000 UTC, the location where and timing when the strongest convection occurred.

The 1800 UTC cycle included new temperature and moisture information obtained from the 1600, 1700, and 1800 UTC GOES sounding scans. The analysis of low-level θ_e , upper-level θ_e and θ_e difference all matched well with the 1500 UTC three hour forecast (Fig. 8). The maximum in low-level θ_e , which was positioned in north-central Kansas at the analysis, was still predicted to move north-northeast into eastern Nebraska by 2100 UTC. Drier air aloft was also still projected to overlay the low-level moisture maximum in eastern Nebraska from the west-southwest leading to the rapid destabilization of a previously stable atmosphere and favorable shear in eastern Nebraska and northwest Iowa where convection developed between 2100 UTC and 0000 UTC. The destabilization

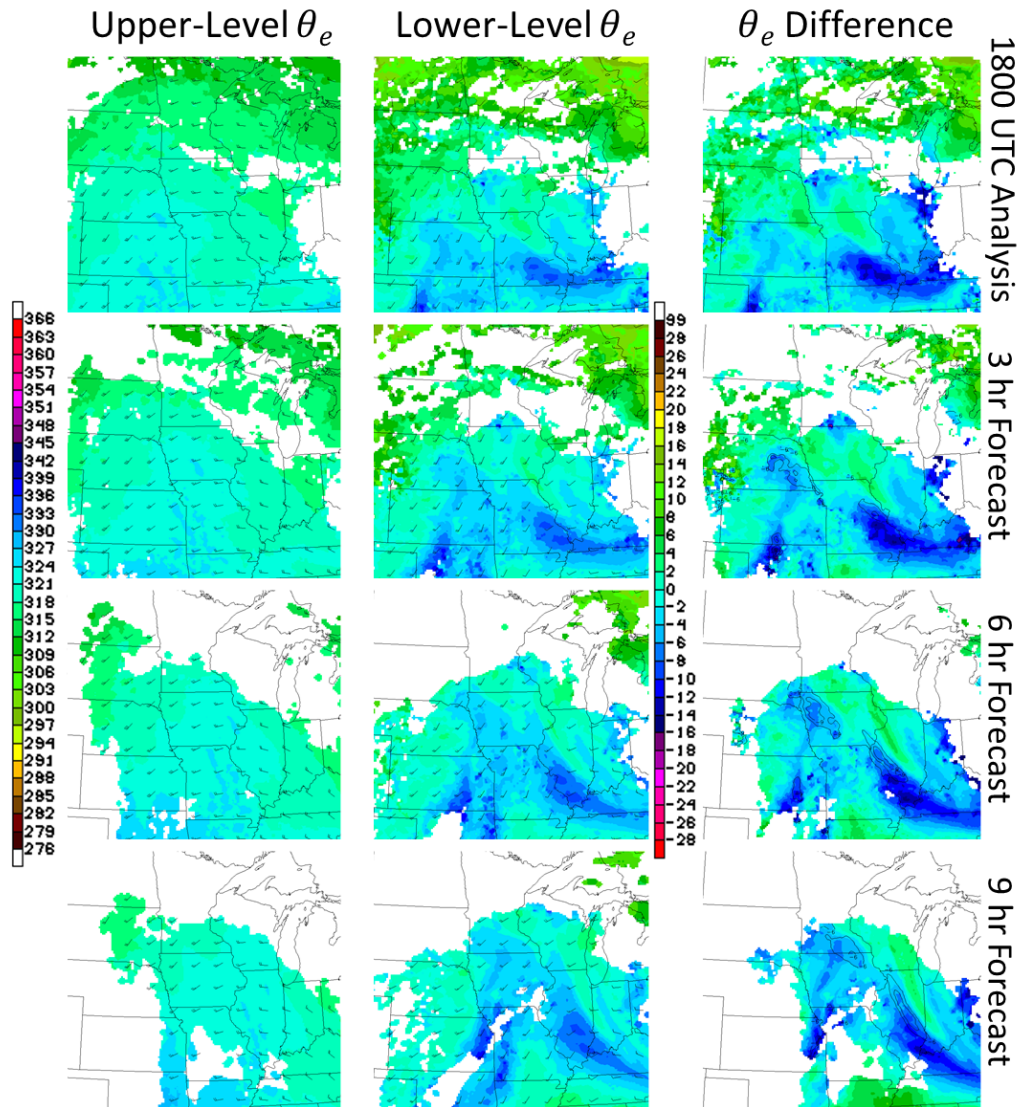


Figure 8: Same as Fig. 7, but for 1800 UTC.

tendencies increased to a maximum of over $-9 \text{ K}/2 \text{ hr}$ in northwest Iowa at 0000 UTC before weakening later in the forecast.

The nine hour NearCast from the 1800 UTC cycle, valid at 0300 UTC, had the highest low-level θ_e air turning to a more westerly track, shifting below moister air at the upper levels as it moved into southeast Minnesota. This weakened the veering

wind profile and caused the region ahead of the instability maximum to gradually become convectively unstable. Areas were no longer stabilizing before the destabilization, decreasing the destabilization tendencies. These details may have contributed to the second round of convection that developed in southeast Minnesota being less severe. The reason why the secondary convection produced much more widespread heavy rainfall than the initial area of severe convection was, however, unclear from the isobaric version of the NearCast model.

Stepping ahead another three hours to the 2100 UTC NearCast analysis, the location (eastern Nebraska) of the low-level moisture maximum, upper-level dry air boundary, and resulting strongest instability were consistent with what was predicted in the 1800 UTC three hour and 1500 UTC six hour forecasts (Fig. 9). The magnitudes of these fields, however, were noticeably different. The dry air boundary at 500 hPa was more distinct, with much drier air moving into eastern Nebraska from the west, while at 780 hPa, the maximum in θ_e was over 10 K warmer than in previous runs. A reason for the increase in θ_e later in the day was likely due to a deepening of the boundary layer and associated warming and moistening of the layer being observed by GOES. Another reason for higher θ_e values later in the day is that the retrievals tend to have a wet bias in the afternoon during the warm season. The patterns in the forecasts were still the same, though, as the atmosphere over northwest Iowa was still forecasted to destabilize quickly (-18 K/2 hr) after a period of stabilization between 2100 and 0000 UTC. Significant speed and directional shear were also still apparent in the region.

Between 0000 and 0300 UTC, the instability maximum was predicted to progress

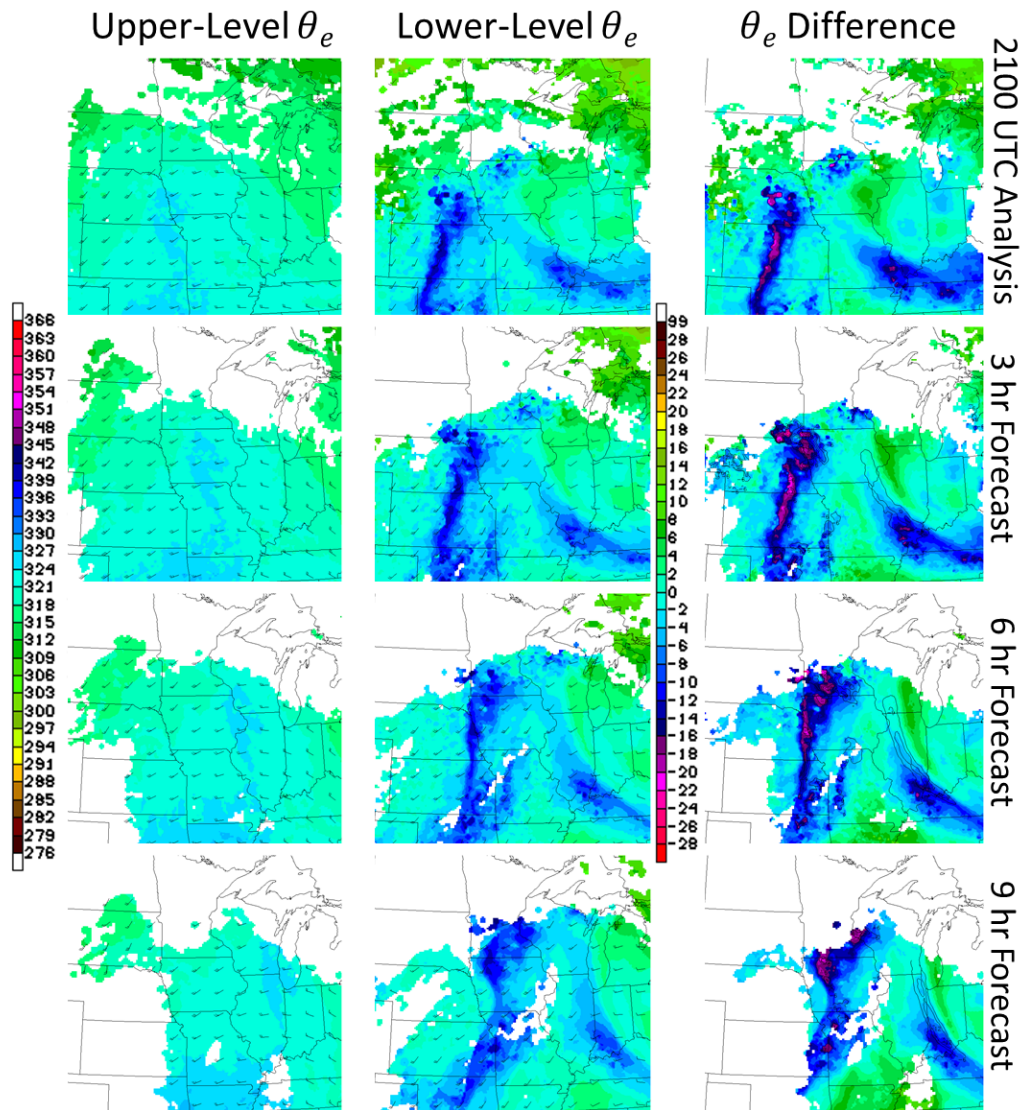


Figure 9: Same as Fig. 7, but for 2100 UTC.

into north-central Iowa, the observed path of convection. By about 0300 UTC, the severe part of this weather event had ended and the initial severe convection was dissipating. Between 0300 and 0600 UTC, the low-level moisture maximum turned to a more westerly track, leading to less of a veering wind profile and weaker destabilization tendencies (-12 K/2 hr) from southeast Minnesota into western Wisconsin, as was seen

in the 1800 UTC cycle. Once again, these changes corroborated the notion that the widespread convection later in the period would be less severe.

The similarities between the 1500, 1800 and 2100 UTC model cycles in depicting the location of the instability maximum and greatest destabilization tendencies are shown in Fig. 10. Each of the three cycles predicted northwest Iowa to be convectively stable at 2100 UTC before becoming convectively unstable by 0000 UTC, resulting in strong destabilization tendencies. All of the cycles also predicted the winds to veer and increase in strength with height over the same location. Consistency between model runs like that seen in this case gives confidence that that the model forecasts will be correct.

In addition to the isobaric model's inability to predict the strength of precipitation to occur with convection, it also does not provide information about the lifting of moisture in the atmosphere which is helpful for convective initiation. These two drawbacks are resolved by running the model in an isentropic framework, discussed in the next subsection.

There are several key points that should be highlighted regarding the isobaric NearCast output: 1) the model is useful in identifying areas where the atmosphere will become convectively unstable [where warm, moist air (high θ_e) is superposed by cool, dry air (low θ_e)] 2) convection develops in maximums of negative θ_e difference, or instability, 3) convection is most likely to occur and be strongest in areas that see the most rapid destabilization tendencies and 4) the prediction of wind shear may be useful in determining the type and strength of the convection.

These points are consistent with evaluations of the isobaric NearCast model made

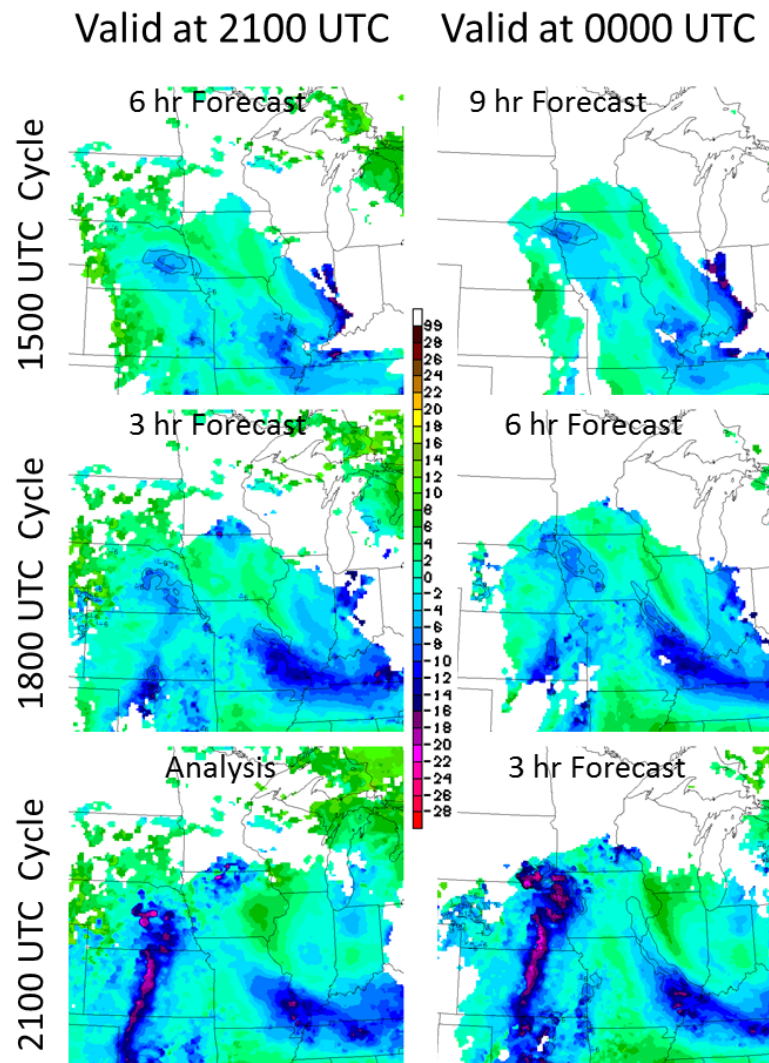


Figure 10: Comparisons of convective instability between the 1500, 1800, and 2100 UTC NearCast forecasts valid at 2100 and 0000 UTC on April 09, 2011.

at the GOES-R Proving Ground activities which took place at the Aviation Weather Center’s (AWC) Aviation Weather Testbed (AWT) and the SPC’s Hazardous Weather Testbed (HWT). Some forecaster feedback from hands-on use of the model output includes:

- “... there was a strong θ_e gradient that the storm was moving into and that gave

- me confidence in that the storm would intensify.”
- “... it was indicative of finding areas of greatly deep instability, or moisture source regions.”
 - “Could clearly see the boundary between the more stable air and unstable air.”
 - “The θ_e difference picked up nicely on the fact that there were stronger signals in N. MI and that correlated well to the stronger storms”
 - “I used it both as a forecast tool and an analysis tool.”
 - “... the instability kept showing up to the SE and I had some confidence that the storms would continue to maintain as they moved through the area.”
 - “... it really had a clear picture of the gradient of moisture and showed a strong push of cooler/dryer air where storms did not end up forming.”

5.2 April 09, 2011-Isentropic NearCast

The April 09, 2011 Mapleton Iowa tornado case will now be examined using the isentropic version of the NearCast model. As discussed earlier, computing trajectories for the satellite sounding observations in an isentropic framework (as opposed to isobaric) provides a more accurate depiction of how they move in an adiabatic atmosphere, since the observations are made from the clear sky, where flow is mostly adiabatic. It is hypothesized that the isentropic version of the model will make more accurate predictions about the movement of moisture within each layer, as well as the layer stability

and shear. It will also add information about adiabatic lift in the deep layer and total layer moisture. The added and more accurate information in the isentropic model will prove to be useful in making better predictions about the timing, location, and type of convection that may occur in the near future.

The 312 K isentropic surface served as the lower level in this case, while the 318 K isentropic surface was the upper level. These levels were chosen based on their respective close proximities to the lower and upper pressure levels where the GOES weighting functions indicate independent moisture information. Since the movement of air parcels along an isentropic surface can be through pressure surfaces, isobars are added to the plots of θ_e to make the three-dimensional movement of the satellite observations through the atmosphere apparent. New parameters derived from running the model in the isentropic framework will be explained throughout the case analysis.

Attention is, once again, first turned to the 1500 UTC run, or approximately 7.5 hours before the onset of convection in eastern Nebraska (Fig. 11). Just like in the isobaric model, a low-level θ_e maximum was located in central Kansas at the analysis time. The θ_e pattern, however, was more continuous and the source region of the moisture (Texas, not shown) was more apparent. The θ_e maximum originated just below 750 hPa, close to the 780 hPa level that was used as the lower level in the isobaric model. The maximum was not forecasted to move along the pressure surface (as in the isobaric model configuration), but was instead projected to move upward in the atmosphere as it advanced northward. This adiabatic lifting of the θ_e maximum along the 312 K surface throughout the forecast period was indicated by the strong

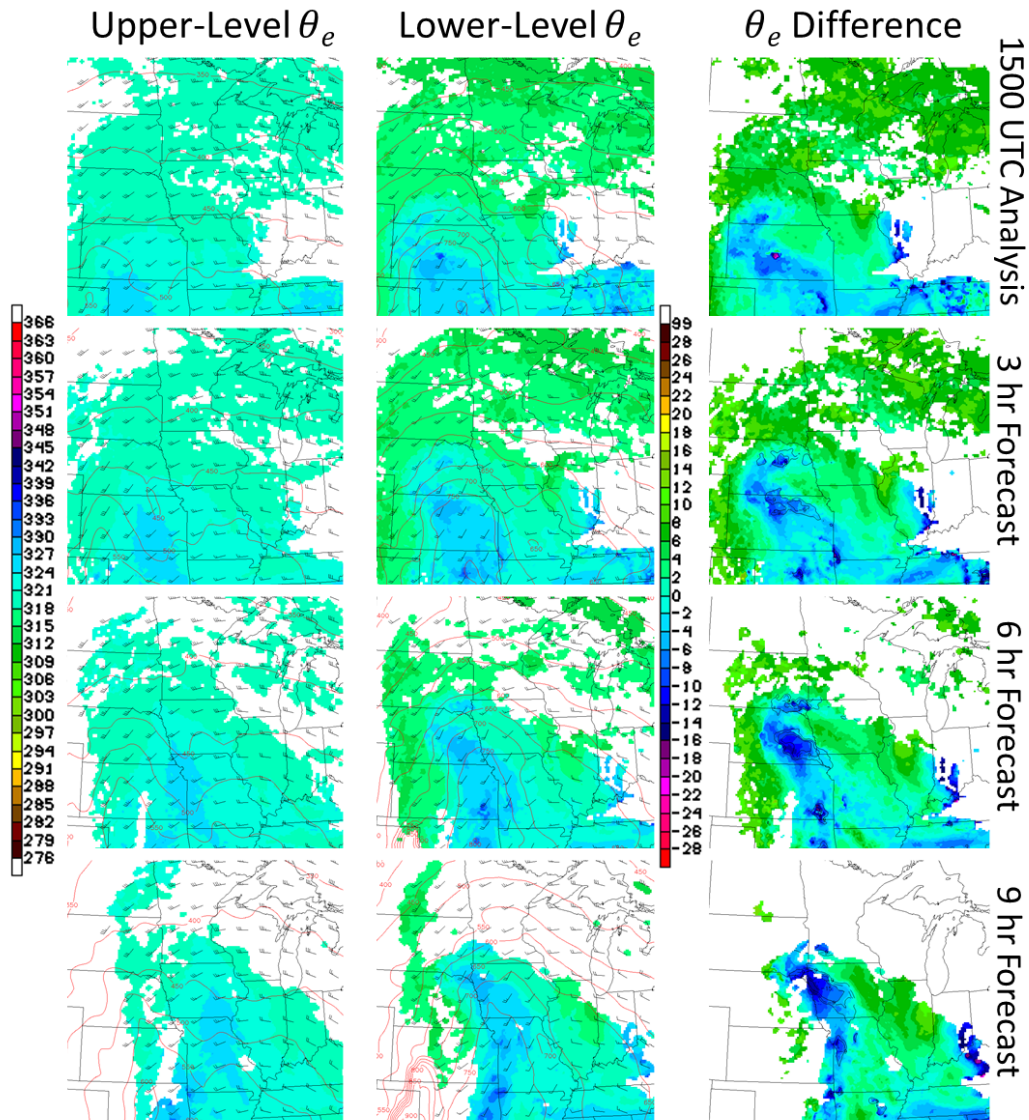


Figure 11: 1500 UTC April 09, 2011 isentropic NearCast model cycle. Similar to Fig. 7, but with trajectories along constant isentropic surfaces as opposed to isobaric ones. Upper level is 318 K , lower level is 312 K, red contours are pressure in hPa. See text for details.

cross-isobaric flow toward lower pressure. By 0000 UTC, the low-level θ_e maximum was predicted to have moved to above 700 hPa in northwest Iowa, an ascent of close to 100 hPa during the nine hour span. This upward flow suggested the presence of a

triggering mechanism for convection, and increased the likelihood that the bottom of the layer would become saturated. More detailed analysis of the vertical motion fields are presented later.

At the 318 K isentropic surface, adiabatic flow continued to have an upward component throughout much of the domain over the forecast period. The deep layer of ascent further supported the potential for convection. Also apparent at the upper level was the forecasted movement of much drier air from the west into eastern Nebraska between 2100 UTC and 0000 UTC. The θ_e gradients were considerably larger on the sloping isentropic surfaces than they had been in isobaric coordinates.

Similar to what was seen in the isobaric version, the stability of the atmosphere is gauged in the isentropic NearCast model by looking at the θ_e difference between the upper and lower isentropic layers (This is closely related to $\frac{\partial q}{\partial \theta}$, where q is the mixing ratio). Comparing Fig. 11 with Fig. 7, both versions of the 1500 UTC model run had the maximum in instability at roughly the same horizontal locations throughout the cycle. The feature, however, became more convectively unstable throughout the isentropic cycle than in the isobaric cycle due to the more accurate depictions of a stronger upper-level dry air boundary and movement of low-level moisture. Consequently, more rapid destabilization tendencies were predicted from eastern Nebraska into northwest Iowa becoming maximized at $-15 \text{ K}/2 \text{ hr}$ between 2100 and 0000 UTC, precisely the time and location of the strongest convection. The isentropic model also predicted a more pronounced stabilization in the area of tornadic development before destabilization, indicating an even stronger capping of thermal energy.

As was seen in the isobaric model, strong wind shear was forecasted where convection occurred. The isentropic version depicts this aspect more vigorously though, as it takes into account additional changes in wind shear due to the changing distance between the upper and lower isentropic level at any given location. Also, as the low-level parcels move upward in a baroclinic atmosphere along the isentropic surface, they experience additional acceleration associated with increasing pressure gradient force due to thermal wind relationships, producing the veering winds and increased vertical speed shear. Vertical motion diagnosed from the isentropic NearCast model will be discussed next.

Vertical motion (ω) in isentropic coordinates can be derived from the expansion of the total derivative of pressure, resulting in three terms (Moore, 1987):

$$\omega = \frac{dP}{dt} = \underbrace{\frac{\partial P}{\partial t}}_A + \underbrace{\vec{V} \cdot \nabla_{\theta} P}_B + \underbrace{\frac{\partial P}{\partial \theta} \frac{d\theta}{dt}}_C, \quad (13)$$

where terms A, B, and C are the:

- (A) Local pressure tendency term. The local time derivative of pressure. Represents the up and down movement of an isentropic surface. In the model, this term is computed from the time change in GFS pressure at every grid point on the isentropic surface.
- (B) Advection of pressure on an isentropic surface. Represents the cross-isobar flow along an isentropic surface. Adiabatic ascent (descent) is occurring when flow along the surface is directed from higher (lower) pressure toward lower (higher) pressure. In the model, this is computed from the advection of GFS pressure by the NearCast model-derived winds.

(C) Diabatic heating/cooling term. The result of diabatic processes such as LHR, which force parcels off of their native isentropic surface. Since the observations used in the NearCast model are made from the clear-sky, diabatic processes are at a minimum, so this term is ignored in this study.

The sum of terms A and B reveals the adiabatic vertical motion on the isentropic surface. Negative (positive) values of ω (and each individual term) indicate upward (downward) vertical motion (UVM, DVM).

The 1500 UTC NearCast cycle forecasted strong vertical adiabatic flow (upward and downward) at the 312 K isentropic surface across the Midwest between 1500 and 0000 UTC (Fig. 12). A major reason for the widespread vertical motion was the movement of a warm (high pressure) thermal ridge across the central United States. This resulted in the isentropic surfaces to be lower in the thermal ridge and higher in the colder air behind it and ahead of it. The forecasted pressure tendency term indicated strong downward movement of the surface through 2100 UTC in northwest Iowa. Between 2100 and 0000 UTC, however, the surface began an ascending pattern in eastern Nebraska as the thermal ridge axis advanced east of the area.

The other component of adiabatic vertical motion is the pressure advection along the isentropic surface. The 1500 UTC cycle indicated a broad area of strong negative pressure advection (flow perpendicular to the isobars towards lower pressure) along the northern and eastern edge of the advancing thermal ridge due to significant warm air advection within the warm sector of a synoptic-scale system (Fig. 12). This pattern contributed to a broad region of UVM that stretched from eastern Kansas northward

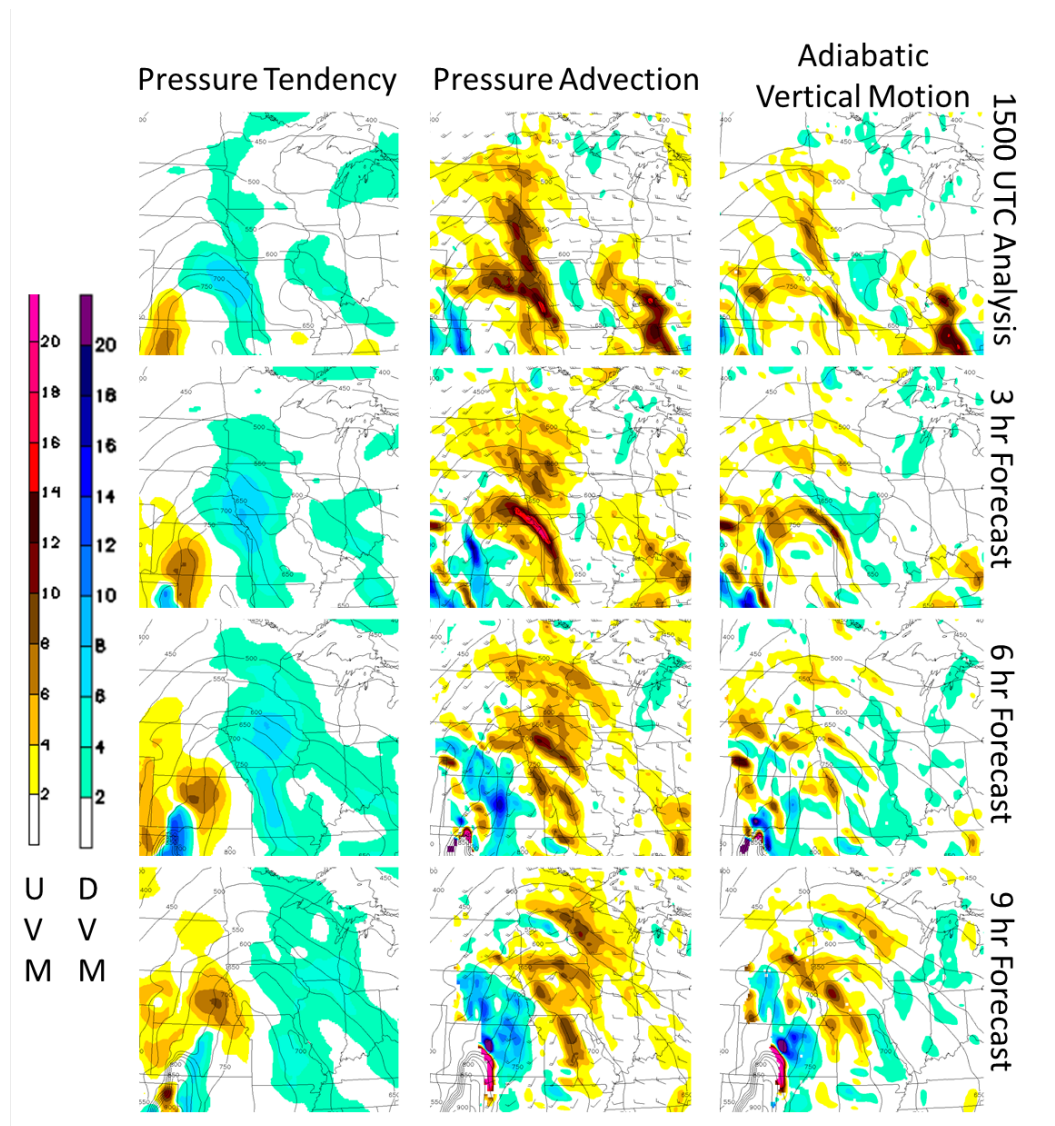


Figure 12: 1500 UTC April 09, 2011 isentropic NearCast model cycle. Adiabatic vertical motion and its two components along the lower (312 K) isentropic surface. Left (right) colorbar is upward (downward) vertical motion. Higher values indicate more rapid vertical motion. Units are $\mu\text{bar/s}$. Interpretation in text.

into South Dakota. It was predicted to slowly shift northeastward with the movement of the thermal ridge during the cycle. Between 2100 and 0000 UTC, the back end of the strongest negative pressure advection was moving into northwest Iowa, with positive pressure advection further to the west.

The sum of the pressure tendency term and pressure advection term is computed so forecasts of the total adiabatic vertical motion at the lower level can be made (Fig. 12). Early in the cycle at forecasts valid between 1500 and 2100 UTC, northwest Iowa was characterized by a DVM contribution from the pressure tendency term, and a strong UVM contribution from the pressure advection term, resulting in weak to moderate total adiabatic UVM. As shown earlier, that same region was forecasted to be stable during this period, so convection was not likely despite the lift. Between 2100 and 0000 UTC, much stronger adiabatic UVM was forecasted in eastern Nebraska and northwest Iowa where rapid destabilization was also predicted. The strong lift at this time was due to a combination of a weak pressure tendency contribution as the thermal ridge axis was moving through the area and a strong pressure advection contribution as parcels were rapidly ascending along the isentropic surface. The forecasted collocation of UVM and rapid destabilization increased confidence that the lower part of the deep layer would become saturated, and convection would develop in eastern Nebraska and move into northwest Iowa between 2100 and 0000 UTC.

Another unique source of information in the observations that is retained by running the model in an isentropic framework is the total mass in each isentropic layer. The layer mass, centered on an isentropic level and averaged over a depth of 2 K, is computed as $\frac{1}{g} \frac{\partial P}{\partial \theta}$, where $\frac{\partial P}{\partial \theta}$ can be thought of as the inverse static stability. Higher (lower) mass per unit kelvin values indicate a greater (lesser) amount of mass in the isentropic layer, weaker (stronger) static stability in the layer, and greater (less) convective potential. Static stability is a simple way of determining the stability of the atmosphere

in isentropic coordinates without considering the effects of moisture (Moore, 1987). In the NearCast model, the total isentropic layer mass term, which is obtained from the GOES temperature soundings, can be used to determine the static stability of a layer.

The total isentropic layer mass term can also be used to determine the total moisture content in an isentropic layer, $\frac{1}{g} \frac{\partial P}{\partial \theta} q_{av}$, where q_{av} is the average mixing ratio in the isentropic layer. Higher values indicate more moisture in a layer, while lower values mean layer moisture is lacking. Interpreting the total layer moisture term, even though a layer may have a high average mixing ratio (high level of moisture), if the layer is very thin, the total moisture content within the layer would actually be quite low. On the other hand, if a thick layer has at least moderate average mixing ratio values measured in it, the total moisture content within the isentropic layer will be high. This total layer moisture parameter can be used to determine whether there is enough moisture to support convective growth, as well as whether a convective event has the potential to produce heavy/widespread precipitation. The model will be used to make predictions about total moisture availability in the lower layer, where moisture fuels sustained convection.

Figure 13 depicts the average mixing ratio in the 312 K isentropic layer at 1500 UTC as measured by the GOES sounder and projected forward in time and space by the NearCast model. Over the nine hour NearCast forecast, a 5 g/kg maximum in mixing ratio was forecasted to move from central Kansas northeastward into northwest Iowa.

At the same time, a strip of relatively high layer mass (weak static stability)

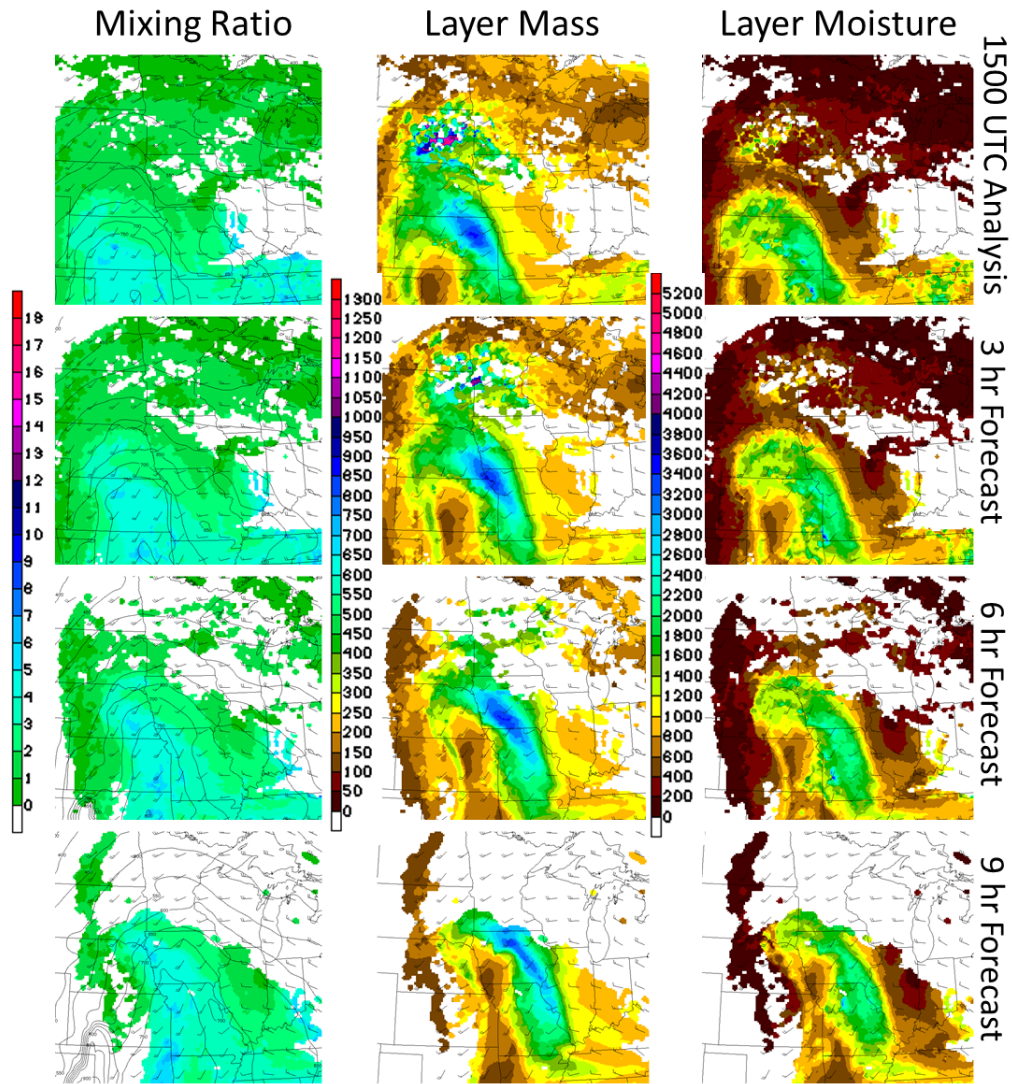


Figure 13: 1500 UTC April 09, 2011 isentropic NearCast model cycle. Average mixing ratio ($\frac{q}{kg}$), layer mass ($\frac{kg}{Km^2}$), and layer moisture ($\frac{q_{moisture}}{Km^2}$) within the lower (312 K) isentropic layer. Interpretation in text.

was oriented just ahead of the moisture maximum as both features advanced north-northeastward (Fig. 13). Between 2100 UTC and 0000 UTC, static stability was forecasted to increase in the layer over eastern Nebraska, with the weakest static stability lying well ahead of the most convectively unstable air. The initial convective

development was confined to the leading edge of the predicted convective instability, where static stability was also weak enough to support convective growth.

Multiplying average layer mixing ratio and total layer mass, the observed and forecasted total moisture content in the lower isentropic layer is revealed (Fig. 13). Total layer moisture was highest where the pocket of highest mass intersected the leading edge of the moisture surge, initially in northeast Kansas. By 2100 UTC, the plume of highest layer moisture was predicted to have already moved through northwest Iowa, advancing into north-central Iowa and toward southeast Minnesota by 0000 UTC, well ahead the strongest convective instability. The lack of heavy/widespread precipitation from the convection that developed within the convective instability maximum in eastern Nebraska was consistent with the smaller amounts of total moisture predicted by the NearCast model. Furthermore, the layer contained enough moisture to support initial convective growth, but not enough to sustain it.

The Isentropic NearCast model cycles initialized between 1500 and 2100 UTC showed much continuity for this event for the θ_e , instability, vertical motion, and total moisture fields, validating each other with each new hour of observations.

In the first three hours of the 2100 UTC Isentropic NearCast cycle, a path from eastern Nebraska to northwest Iowa was still predicted to experience strong destabilization tendencies of $-18 \text{ K}/2 \text{ hr}$, indicating convection was imminent (Fig. 14). UVM along the lower isentropic surface in the same region was even stronger than predicted earlier, providing lift to potentially release the convective instability (Fig. 15). The strip of highest total moisture in the layer was, once again, forecasted to remain just

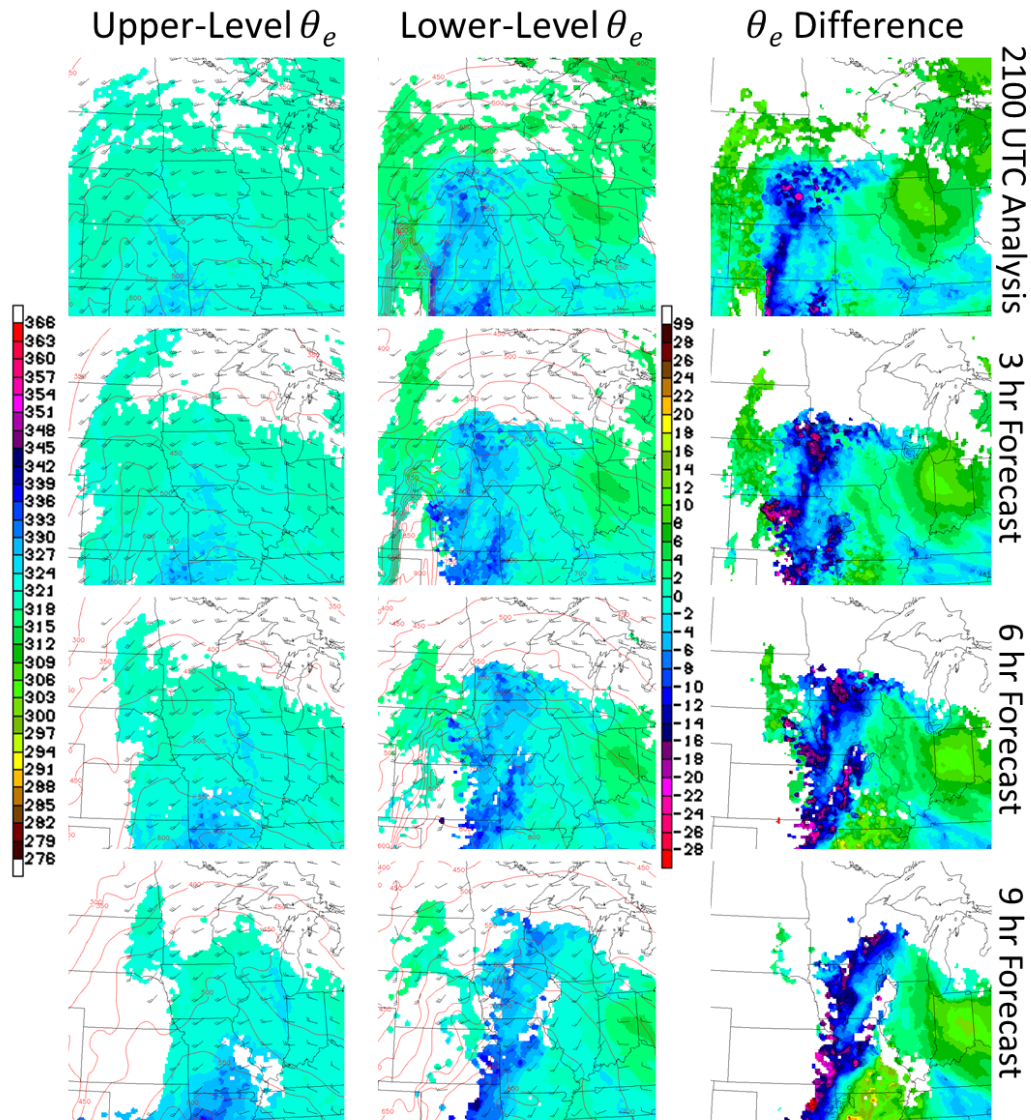


Figure 14: Same as Fig. 11, but for 2100 UTC.

ahead of the instability maximum (Fig 16). All of these clues successfully pointed to the likelihood of severe, dry, and short-lived convection developing from eastern Nebraska into northwest Iowa between 2100 and 0000 UTC.

The 2100 UTC NearCast cycle also provided information to help predict the secondary, longer-lived convection that produced heavy precipitation from southeast Min-

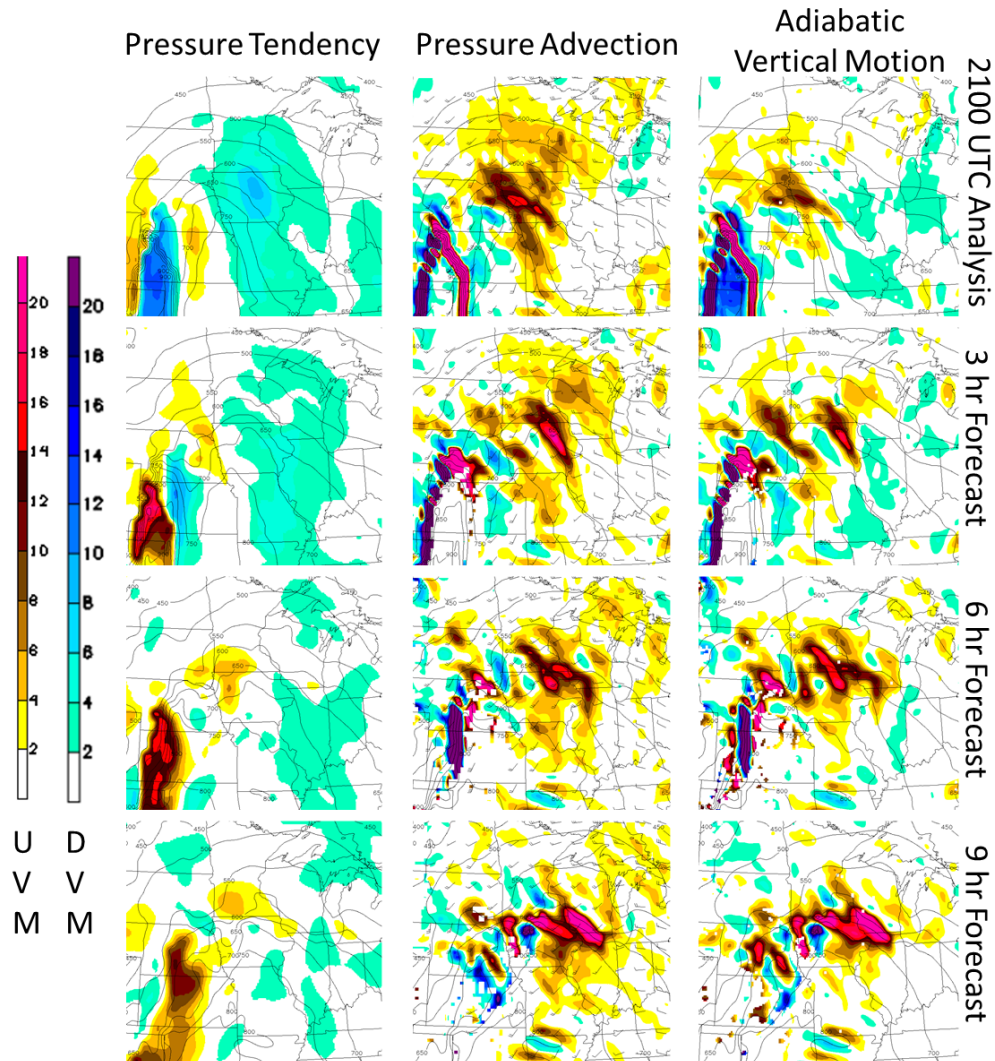


Figure 15: Same as Fig. 12, but for 2100 UTC.

nesota through central Wisconsin. This area of convection developed along Minnesota's southern border between 0200 and 0400 UTC before advancing eastward into northeast Wisconsin by 0600 UTC.

Between 0000 and 0600 UTC, the low-level moisture maximum was predicted by the isentropic model to take on a more westerly track as it moved from southeast Minnesota into western Wisconsin. The dry air boundary at the upper level was still overlaying

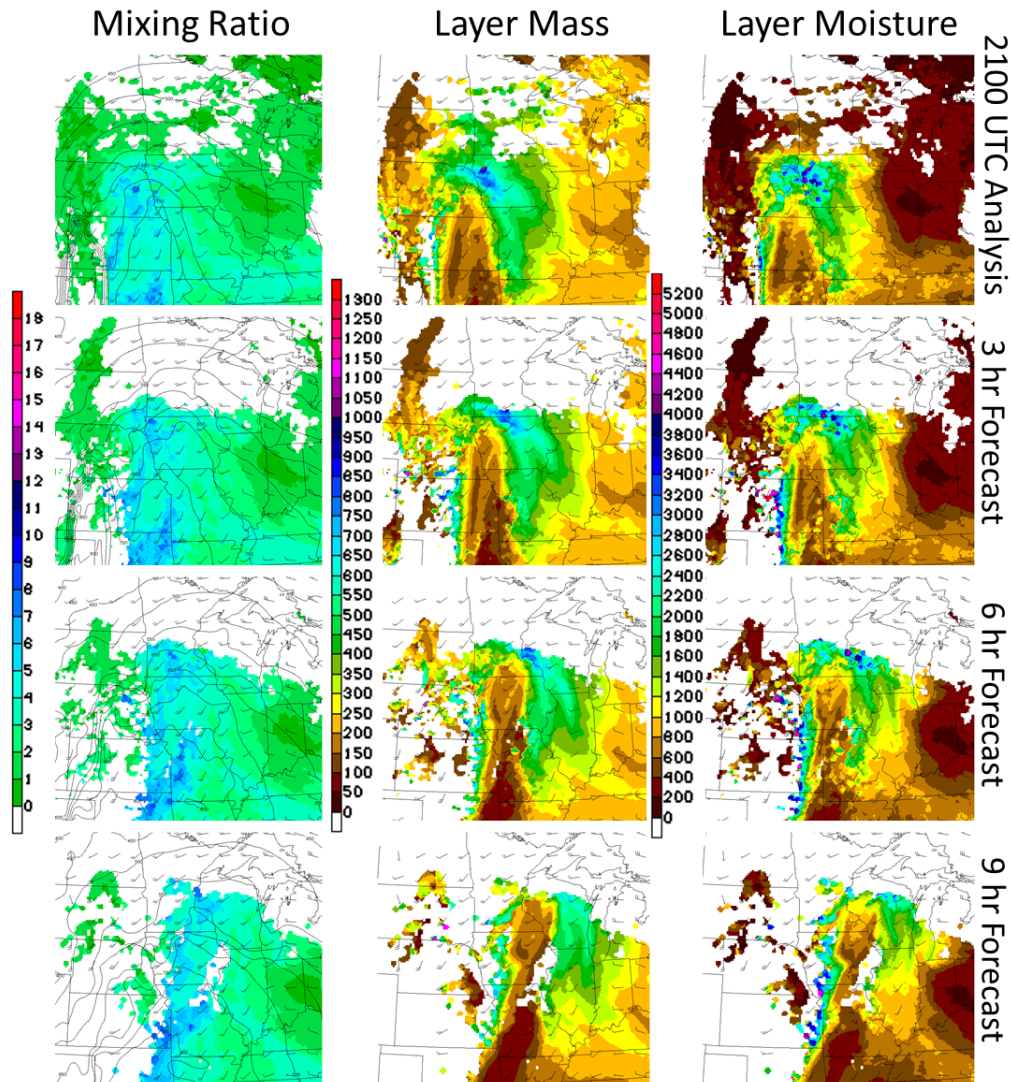


Figure 16: Same as Fig. 13, but for 2100 UTC.

the low-level moisture from the west, leading to destabilization in southeast Minnesota by 0300 UTC. These tendencies were forecasted to be weaker than they were earlier in the cycle because areas ahead of the instability maximum had already experienced gradual destabilization for several hours due to the change in flow at the lower level. Additionally, the shifting low-level winds were causing the wind shear to become much

weaker, further reducing the risk of severe convection. There was, however, ample adiabatic lift in the area of convective instability, as the cross-isobar flow was still quite strong, contributing to the eastward shift of the strongest UVM.

Between 0300 and 0600 UTC in the 2100 UTC forecast, the highest amounts of total moisture in the lower isentropic layer were now well collocated with areas of convective instability and adiabatic lift from southeast Minnesota through much of central Wisconsin. Widespread, longer-lasting convection did indeed develop across this region producing much more precipitation than was seen earlier in eastern Nebraska and northwest Iowa. By running the model in an isentropic framework, the GOES sounding observations were further utilized in a way that the isobaric framework could not. The ability to depict the total moisture content in an isentropic layer proved to be valuable in predicting the degree of precipitation that could occur with convection, and where the heaviest precipitation was most likely.

Summarizing, the extra information made available by running the model in isentropic coordinates instead of pressure coordinates was valuable in making more accurate, detailed forecasts of convection on April 09, 2011. The isentropic trajectories more appropriately moved the observations forward in space and time in three-dimensions, allowing for better predictions of upper- and lower-level θ_e , atmospheric stability, and shear. The ability to forecast lift further narrowed down where convection was most and least likely to occur. By utilizing information about the total moisture content within the lower isentropic layer, predictions were able to be made regarding the degree of precipitation that would occur with convection.

Output from the isentropic version of the NearCast model can be interpolated from isentropic coordinates to be studied on constant pressure levels instead. The interpolation retains the added and more accurate information produced by the isentropic model, while making the output more compatible with other forecasting tools. The interpolated output, however, does not visually showcase the continuous, three-dimensional movement of the observations that is clearly evident when looking at the output in isentropic coordinates.

5.3 June 08, 2011 - Isentropic NearCast

The next case to be discussed occurred on June 08, 2011 across the upper Midwest. Convection began its initial development at 2100 UTC from central Iowa to northeast Wisconsin, quickly growing large (Fig. 17). The broad area of convection sagged southeast into northern Illinois, southeast Wisconsin, and Michigan by 0300 UTC with storms producing severe hail and winds along their path (Fig. 18). Moderate levels of precipitation were recorded in Iowa, Wisconsin, and Michigan, with a particularly heavy swath of rainfall occurring across northern Illinois (Fig. 18, inset). Using the 2100 UTC NearCast cycle, it will be shown that the isentropic model was not only able to correctly predict where convection was most likely to develop and move during the period, but also where the environment was most favorable heavy rainfall. Cycles initialized from 1500 UTC through 2000 UTC (not shown) were consistent in showing the same features that the 2100 UTC cycle (described next) would show, proving to be especially useful in predicting areas of convective instability. The 312 K isentropic

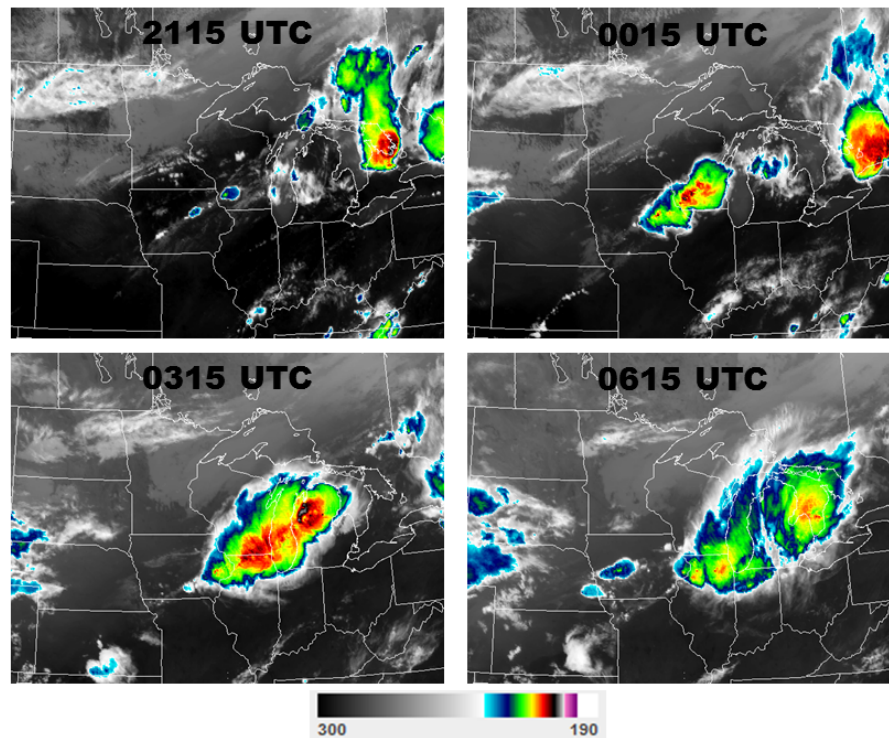


Figure 17: Same as Fig. 5, but for June 08, 2011.

surface is used as the lower level, while the 320 K isentropic surface represents the upper level.

The 2100 UTC NearCast analysis showed a broad plume of warm, moist air stretching from southwest Iowa to northern Lower Michigan (Fig. 19). The moisture plume was forecasted to advance eastward during the period, with much drier air moving into the northern half of Wisconsin from the northwest. At the upper levels, a significantly drier airmass was situated above the low-level moisture feature, with especially dry air forecasted to advance southeastward during the period. The θ_e difference field revealed a long band of instability stretching from Iowa to Michigan with a well-defined transition to stability just to the northwest and weaker instability to the southeast. Adiabatic

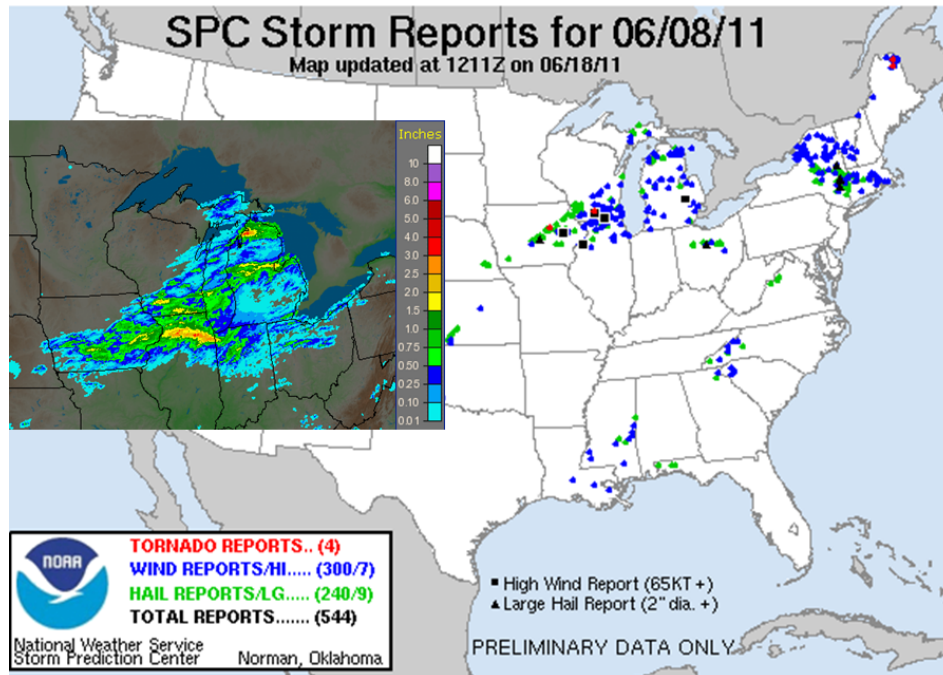


Figure 18: Same as Fig. 6, but for June 08, 2011.

UVM was predicted along the area of instability, with the strongest ascent located in the southern half of Wisconsin (not shown).

Convection developed within the strip of greatest convective instability and UVM, moving southeastward through the period and staying within the forecasted instability. No convection formed to the northwest where the atmosphere was forecasted to be convectively stable, or to the south where the layer was only weakly destabilized. This case displayed the usefulness of the NearCast model in isolating the movement of convection that is already developed or is in the early developmental stages.

The total moisture fields helped to further narrow down where convection was most and least likely to thrive, and helped to correctly predict the degree of precipitation that would occur. At 2100 UTC, very moist air was in place throughout the region within

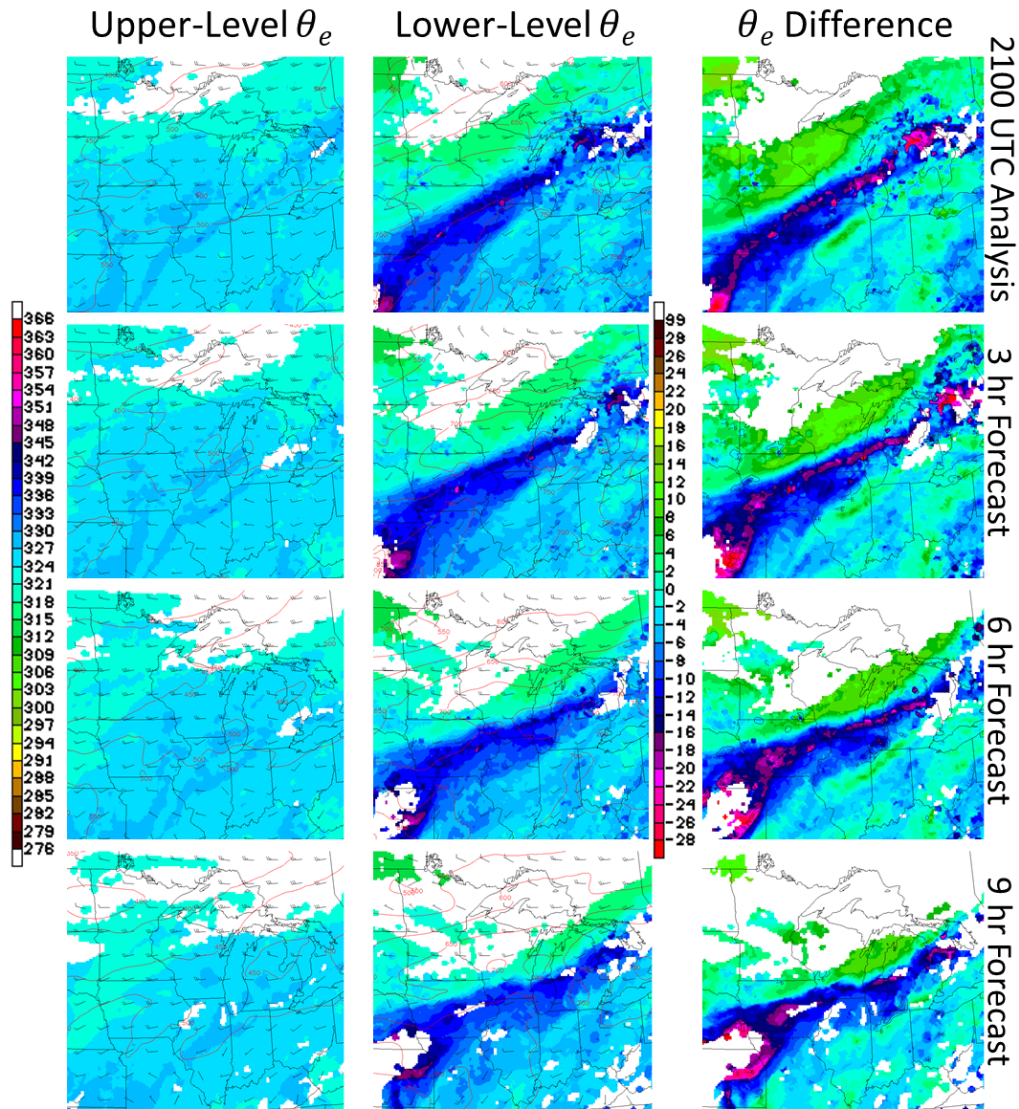


Figure 19: Same as Fig. 11, but for 2100 UTC June 08, 2011. Upper level is 320 K, lower level is 312 K.

the lower level, matching well with the plume of high θ_e air at the same level (Fig. 20). The total layer mass parameter indicated moderate values across southern Wisconsin into Michigan, while the layer was much thinner to the north and southwest. There was a bubble of significantly higher mass values located over the Iowa-Missouri-Illinois tri-state border.

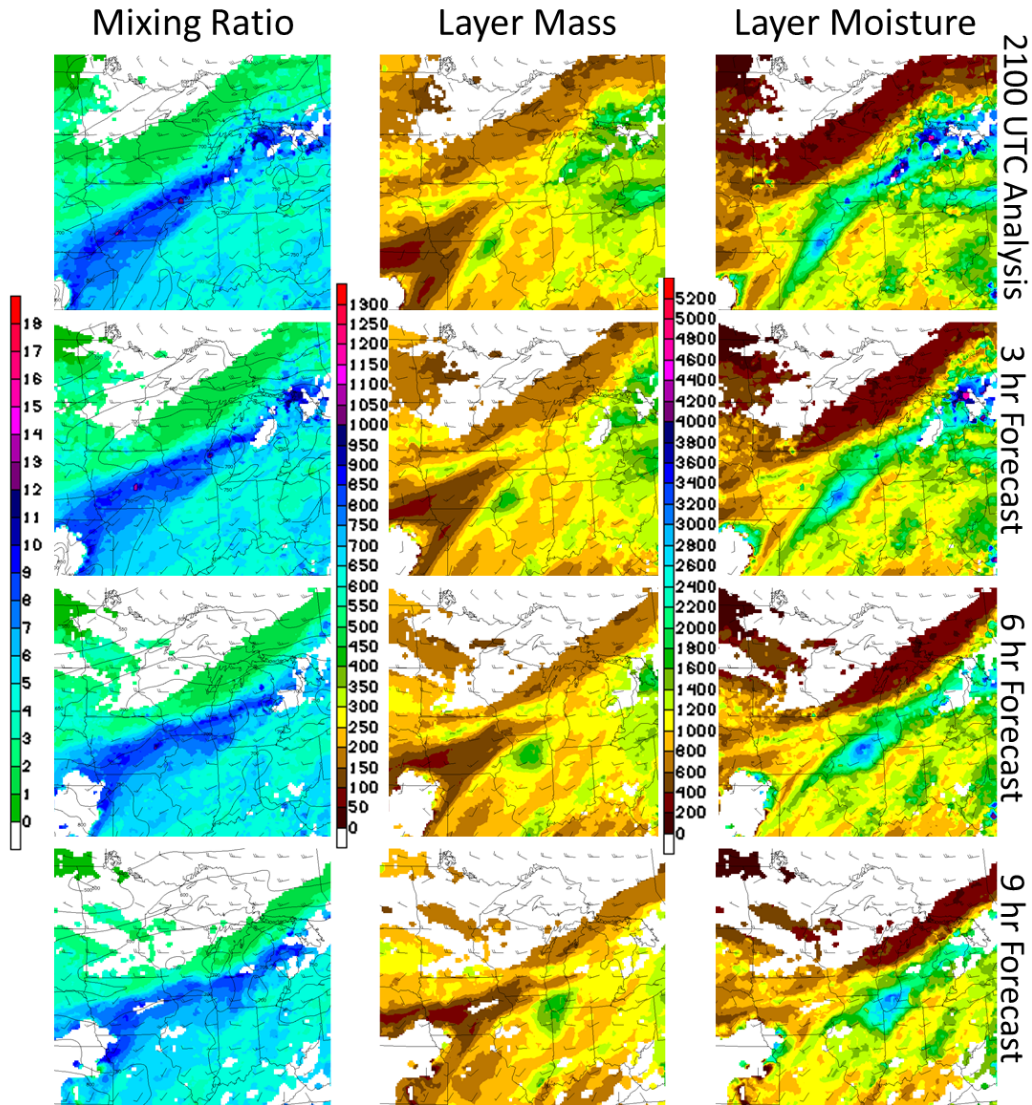


Figure 20: Same as Fig. 13, but for 2100 UTC June 08, 2011. Upper level is 320 K, lower level is 312 K.

Multiplying the total mass and mixing ratio together revealed a broad region of moderate total moisture content in the lower layer from southern Wisconsin into Michigan. Its forecasted movement was collocated with the movement of the strongest instability from southern Wisconsin into northern Lower Michigan, where convection grew and produced significant rainfall totals. In the southwest part of the domain, however, the

highest amounts of layer moisture was oriented south of the strongest convective instability, perhaps a reason why convection had difficulty developing in southwest Iowa and Kansas, where only light rainfall occurred.

The highest total layer moisture amounts were initially located over the tri-state region mentioned earlier, where moderate mixing ratio values were collocated with a bubble of high layer mass. This feature was projected to move northeast through northern Illinois and over the southern tip of Lake Michigan by 0600 UTC, where the atmosphere was also predicted to be convectively unstable. The convection that formed over this forecasted lower-layer moisture maximum produced the heaviest and most widespread rainfall seen with this event, owing to the abundance of low-level moisture. This case was another example of how the isentropic NearCast model can be quite useful in predicting where heavy precipitation is likely to occur.

5.4 June 01, 2011 and May 29, 2012 - Isentropic NearCast

The final two cases to be discussed occurred on June 01, 2011 and May 29, 2012, both in New England. These cases are discussed in tandem due to their many similarities but relevant differences.

Starting with the June 01, 2011 case, a line of thunderstorms began development in New York around 1500 UTC with convection strengthening and expanding along a southwest to northeast boundary as it shifted eastward through the New England states, reaching the coast by 0000 UTC (Fig. 21). The convection stayed confined to the boundary, never growing exceptionally large or organizing together. There was

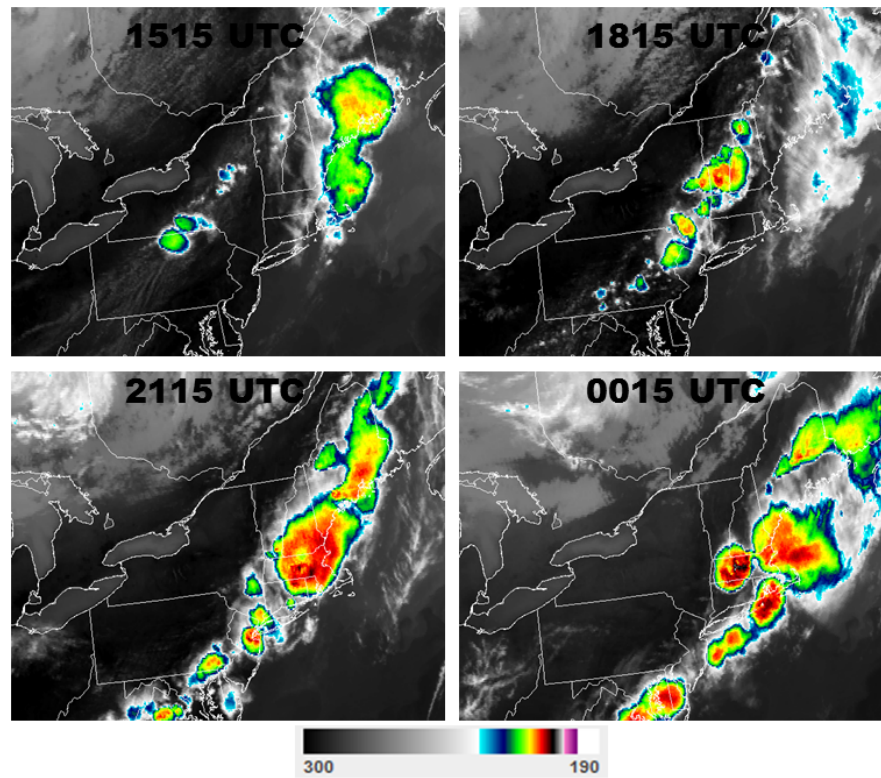


Figure 21: Same as Fig. 5, but for June 01, 2011.

localized severe weather associated with some of the storms including hail, winds and a few tornados (Fig 22). The strongest convection passed through Massachusetts between 2100 and 2200 UTC, producing a large tornado which killed at least 3 people and injured over 70 others as reported to the SPC. Despite the severity of the convection, precipitation amounts were quite low, with only a few very localized areas recording considerable rainfall (Fig 22, inset).

The NearCast cycle initialized at 1500 UTC provided information that was valuable in forecasting the development of convection in New England, its movement, and the degree of rainfall that would occur. At the analysis time, there was an apparent θ_e

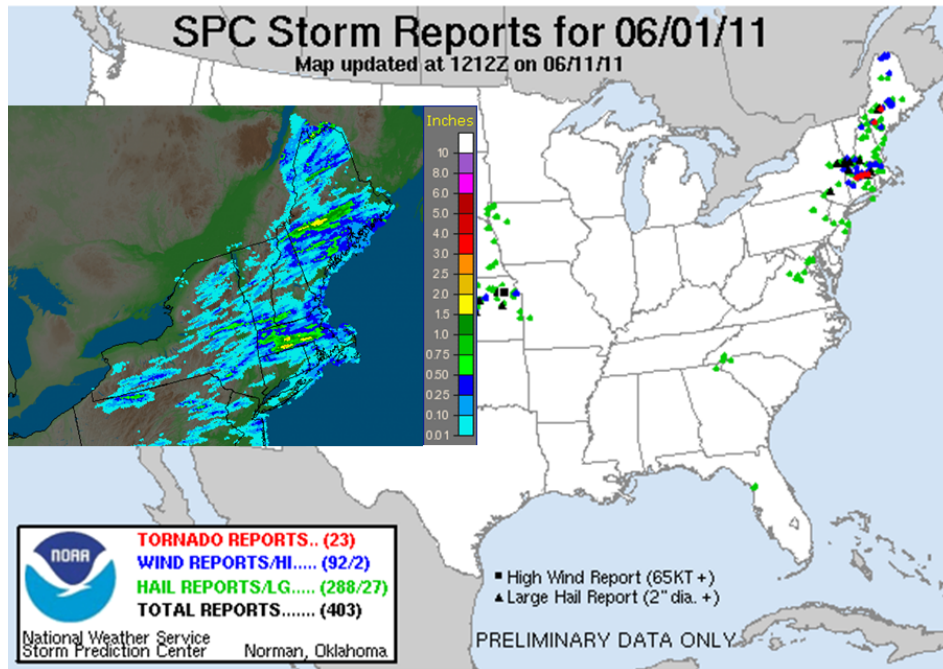


Figure 22: Same as Fig. 6, but for June 01, 2011.

boundary at the 310 K lower level stretching from western Pennsylvania northeast into Quebec (Fig. 23). A drier and cooler airmass lay west of the boundary, while the atmosphere to the east was warm and moist, with highest θ_e values along the leading edge of the boundary. At the 320 K upper level, θ_e values were uniformly lower throughout the region, with a weak dry air boundary located in central New York above the low-level moisture boundary. This setup correlated to a southwest to northeast line of relatively strong convective instability, with very convectively stable air to the west, and weak convective instability to the east.

The forecasted movement of the moisture boundary at both levels was westerly, indicating weak shear. Correspondingly, the instability strip along the boundary was shifting eastward throughout the forecast, reaching the coast by 0000 UTC. Convection

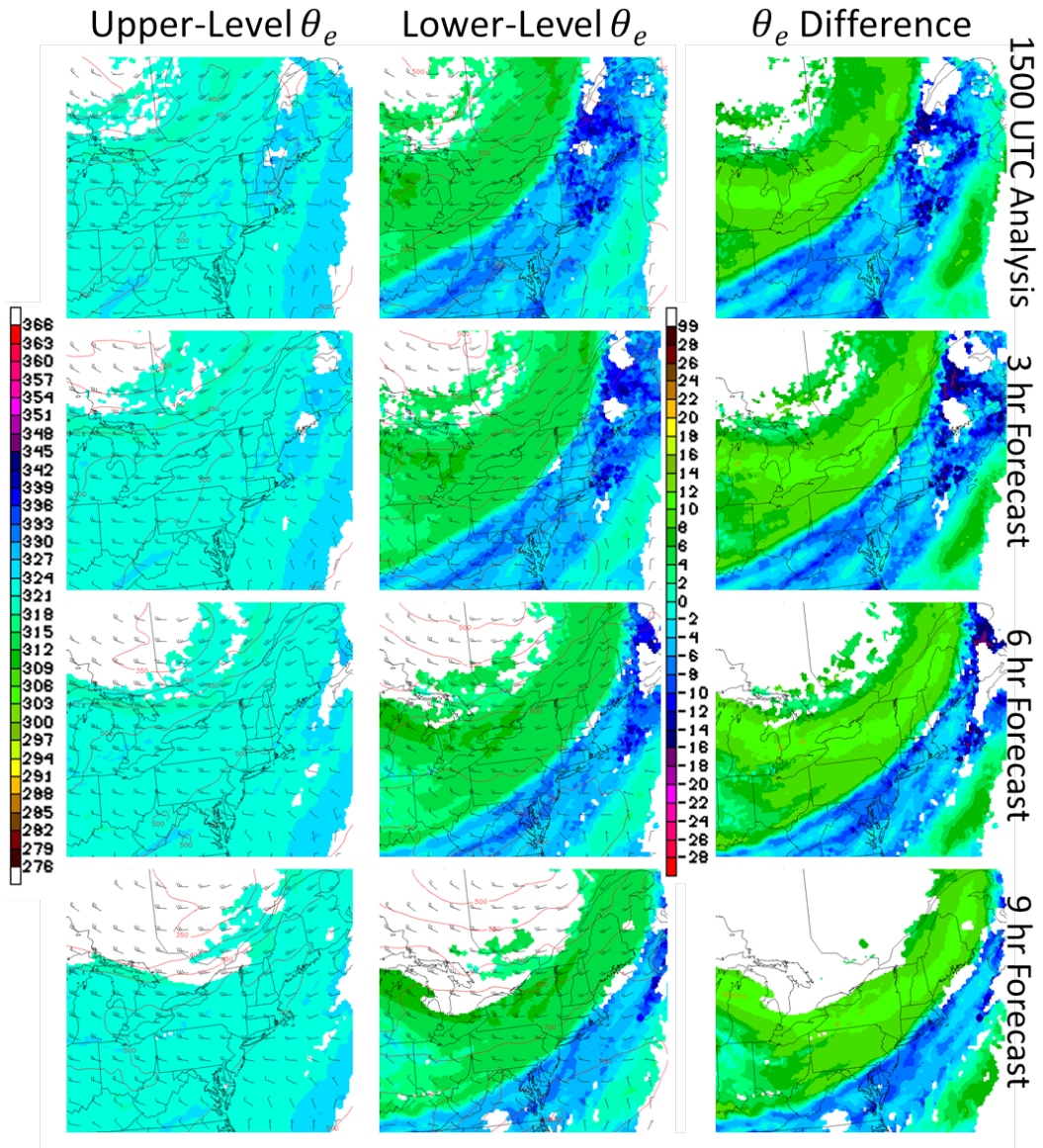


Figure 23: Same as Fig. 11, but for 1500 UTC June 01, 2011. Upper level is 320 K, lower level is 310 K.

advanced eastward with the forecasted movement of the boundary, staying within the strip of greatest instability. The weak dry air boundary at the upper levels was forecasted to advance over the low-level moisture maximum by about 2100 UTC in Massachusetts, correlating to a localized maximum in convective instability and relatively strong destabilization tendencies. The strongest convection in this outbreak formed

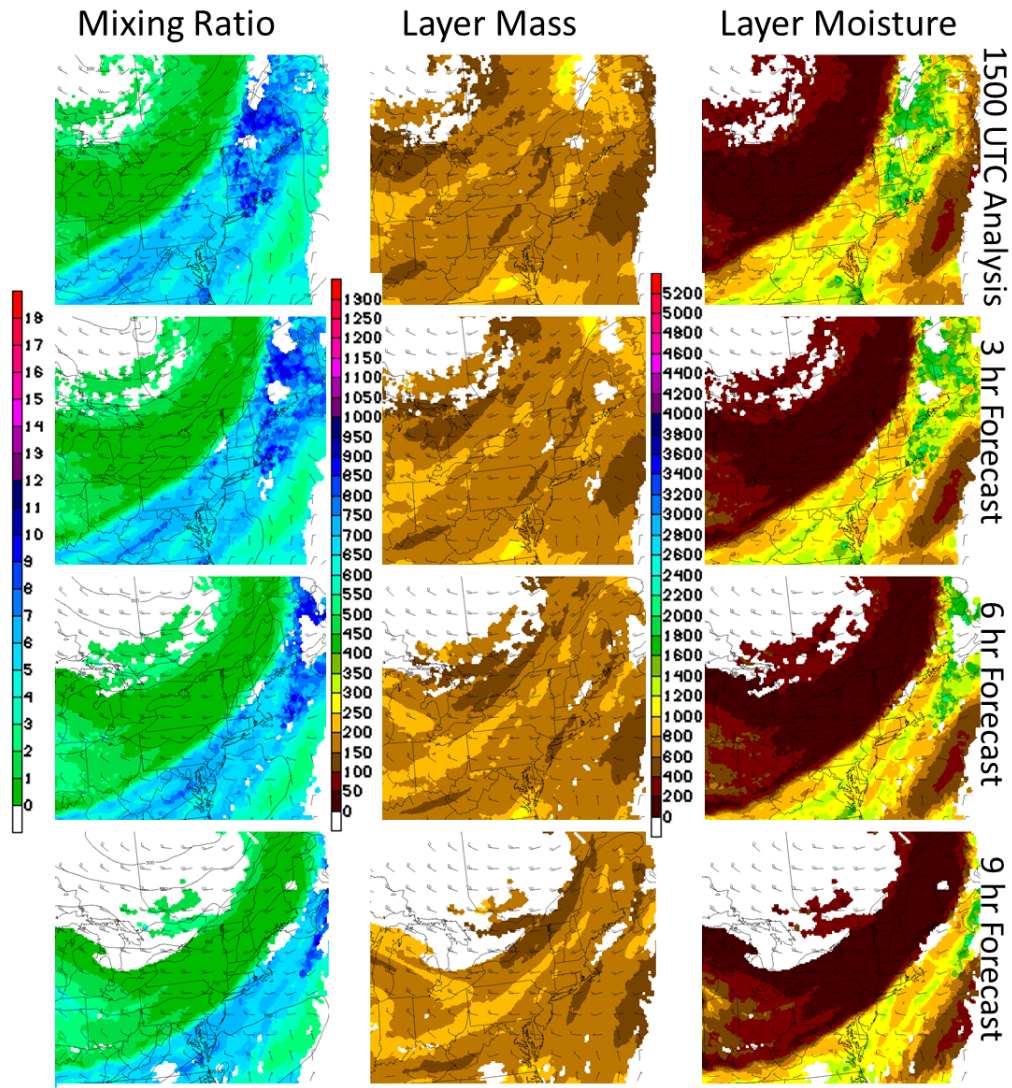


Figure 24: Same as Fig. 13, but for 1500 UTC June 01, 2011. Upper level is 320 K, lower level is 310 K.

within the forecasted instability maximum as it passed through Massachusetts between 2100 UTC and 2300 UTC, producing the deadly tornado. The lack of exceptionally strong and organized storms was likely due to the minimal shear, weak destabilization tendencies, and lack of low-layer moisture, which is discussed next.

The total mass and moisture fields in the lower layer for the 1500 UTC cycle showed

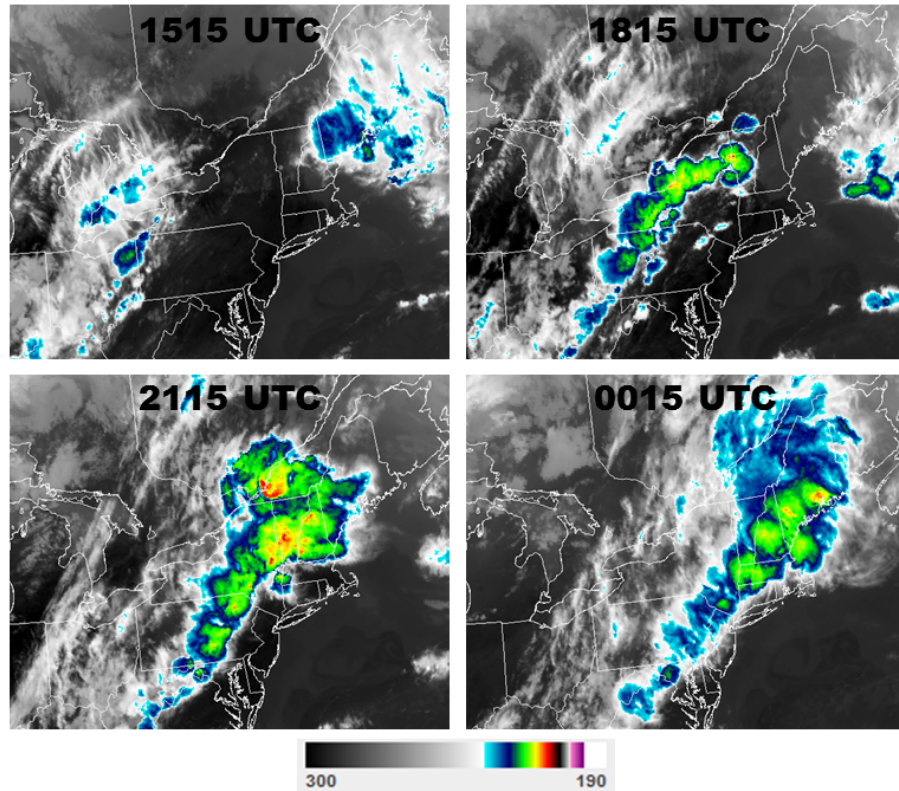


Figure 25: Same as Fig. 5, but for May 29, 2012.

the dry air boundary that was distinct in the θ_e fields (Fig. 24). Although the mixing ratio was relatively high within the layer ahead of the boundary, the isentropic layer was very thin, resulting in low values of total layer moisture and high static stability. As a consequence of the lack of total moisture in the lower layers, the convection never became well organized or widespread, and precipitation totals across the region were light. The NearCast model successfully predicted that total moisture in the lower layers would not be sufficient for any widespread significant rainfall to occur.

The May 29, 2012 case was similar to the previous case in that a line of convection formed along the western borders of Pennsylvania and New York at 1500 UTC,

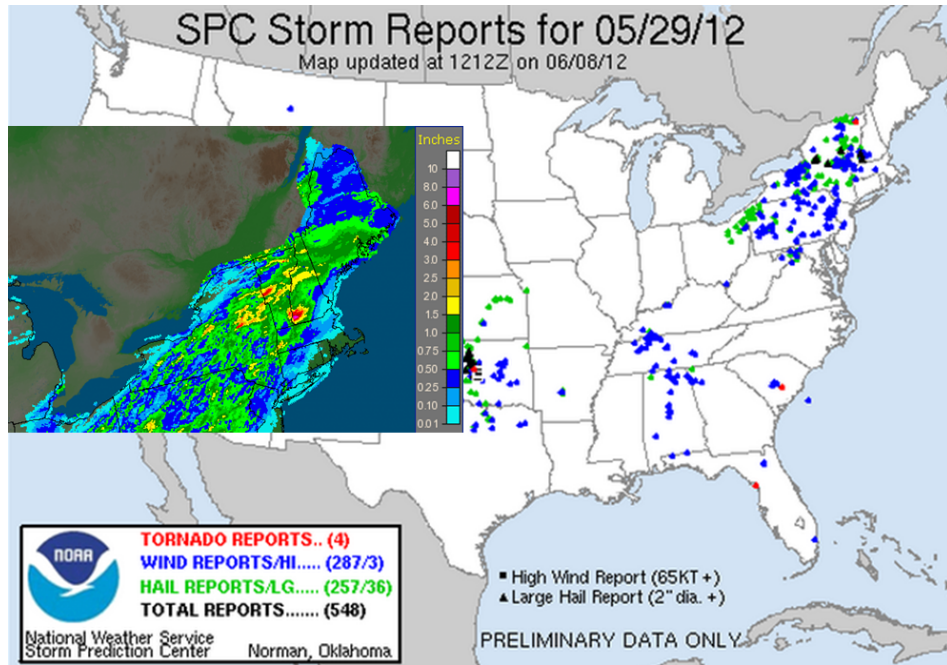


Figure 26: Same as Fig. 6, but for May 29, 2012.

strengthening and moving eastward to the Atlantic coast by 0000 UTC (Fig. 25). Severe weather was reported throughout the region with this line of storms (Fig. 26). The convection, however, was more organized than that in the previous case, producing heavy and widespread rainfall throughout the region, with especially high amounts across eastern New York, Vermont and New Hampshire (Fig. 26, inset).

The 1500 UTC NearCast cycle was similar to that seen with the previous case (Fig. 27). At the 308 K lower level, there was a distinct θ_e boundary stretching southwest to northeast throughout the northeastern United States, with a band of relatively high θ_e air preceding drier air to the west. At the 318 K upper level, the air above the θ_e maximum was significantly drier, yielding a region of instability ahead of a stable airmass. The line of highest convective instability was predicted to shift

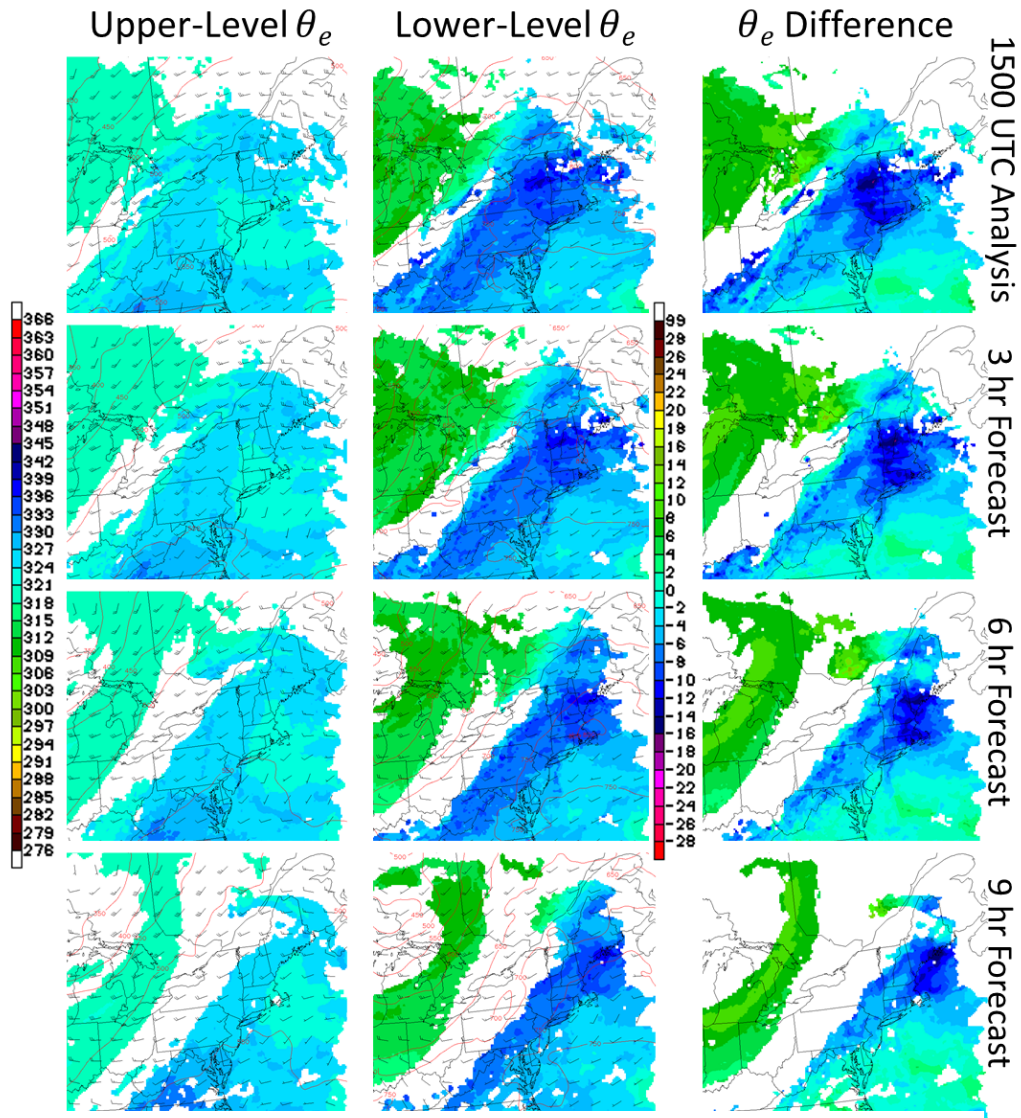


Figure 27: Same as Fig. 11, but for 1500 UTC May 29, 2012. Upper level is 318 K, lower level is 308 K.

east-northeastward during the period, with very little shear between the two levels. Once again, the convection developed and stayed within the forecasted movement of strongest instability for the duration of this event.

The main difference between these two cases came with the forecasted total moisture in the lower layers (Fig. 28). With the May 29 case, the layer contained significantly

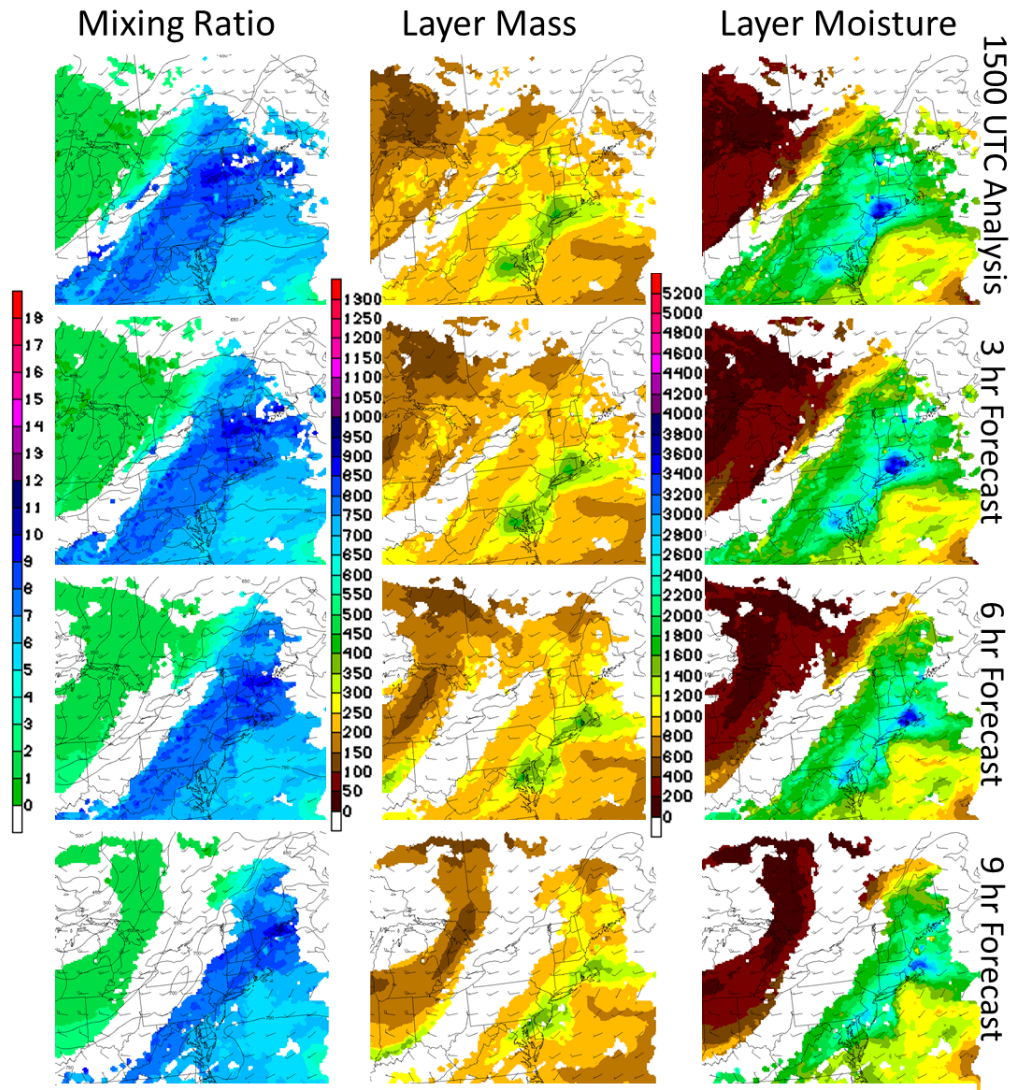


Figure 28: Same as Fig. 13, but for 1500 UTC May 29, 2012. Upper level is 318 K, lower level is 308 K.

higher amounts of total moisture than in the June 01 case. The total moisture amounts feeding the area of most convectively unstable air were similar to those seen with the April 09 and June 08 heavy precipitation cases described earlier. With the added availability of moisture in the low layer, convection was more widespread and organized, leading to higher amounts of precipitation recorded throughout the region.

The ability to contrast these two events in terms of precipitation was not a simple option using the isobaric version of the model. The isentropic NearCast model allowed for the analysis and prediction of total moisture being transported by the dominant adiabatic processes, and therefore, provided useful information about the degree of precipitation that would occur.

6 Summary and Conclusions

NWP performance in the short-term prediction of precipitation is an area that needs improvement, especially in the warm season. A key reason for the poor model performance is often the inability to resolve small mesoscale features such as convection. One source of detailed information about the pre-convective environment is the GOES sounder, which observes the movement of moisture in three-dimensions through the atmosphere exceptionally well. A physical retrieval process uses the radiances measured by the sounder, along with a model first guess, to produce moisture profiles at high temporal and spatial resolution. At the current time, however, the assimilation of this dataset into current NWP is difficult due to biases in the model first guess and high land surface emissivity, which make the retrieval process difficult near the surface. Also, the smoothing of data in current weather models removes important details that are observed well by the satellite such as boundaries, maxima and minima. A new tool to help forecasters improve precipitation and convection forecasts has been developed which uses temperature and moisture data from the GOES sounder.

The NearCast model is an observation-based, Lagrangian trajectory model that dynamically projects the sounding temperature and moisture observations forward in space and time out to nine hours. It takes advantage of the under-utilized moisture retrievals to improve the analysis and short-term prediction of the pre-convective environment. The model predicts where convection is most and least likely to occur by computing trajectories of the observations along multiple levels in the atmosphere. θ_e is computed from the observations allowing for level-to-level comparisons and for the analysis of deep-layer convective instability. Since a Lagrangian framework is used, the model avoids difficulties encountered when assimilating the observations into a Eulerian model. The simple model has quick run times, and there is no smoothing of the observations, allowing for the preservation of fine details in the data. The NearCast model further utilizes every observation by including the previous 10 hours of observations from past model cycles in its analysis and forecast displays, filling in data gaps caused by cloudy skies. Output from the model is available within minutes of the observation times.

The original version of the model computes trajectories along constant pressure surfaces, and has proven that the Lagrangian trajectory approach using satellite observations can be successfully applied to make predictions of atmospheric stability. Since the sounding observations are made from the clear sky where flow is mostly adiabatic, it was hypothesized that their actual movement could be predicted more accurately in an isentropic framework with trajectories along constant potential temperature surfaces. A three-dimensional, isentropic version of the model, therefore, has been developed to

more accurately predict the movement of the observations and to retain more information from them.

The April 09, 2011 Mapleton Iowa tornado and heavy precipitation case in Minnesota and Wisconsin show the extra information gained from running the model in the isentropic framework. For one, by more appropriately predicting the movement of these observations in three-dimensions along isentropic surfaces, the model can 1) depict adiabatic lift, 2) give more details into the shear environment, 3) more accurately predict the movement of θ_e through the atmosphere on each level and 4) provide more accurate predictions of convective instability and destabilization. Secondly, the isentropic model provides extra information from the temperature and moisture observations, including total layer mass and total layer moisture. This information can be used to identify 1) whether there will be enough moisture to support convective growth, 2) the longevity of potential convection and convection that has already formed and 3) whether a convective event will produce heavy rainfall or be relatively dry. The June 08, 2011, June 01, 2011, and May 29, 2012 case studies further demonstrate the advantages of running the model in an isentropic framework.

The NearCast model has been successfully tested over Europe and Lake Victoria using temperature and moisture retrievals from the Spinning Enhanced Visible and Infrared Imager (SEVIRI) instrument, the European advanced imager, similar to the Advanced Baseline Imager (ABI), the future GOES imager. Tests have shown that the higher temporal and spatial resolution observations improve overall data coverage in the NearCast analyses and forecasts.

Future opportunities for improvement and expansion of the NearCast model could include 1) running the model over the Alaska region using hyperspectral data from polar orbiting satellites, which could potentially lead to the use of polar satellite data over the CONUS and 2) developing a version of the model using the terrain-following sigma coordinate as the vertical coordinate at lower levels. Trajectories along a sigma surface would likely be more accurate in regions where terrain has an influence on flow.

Animated graphical displays of experimental NearCast model output are produced hourly (shortly after the observations become available) and can be found on the web at <http://cimss.ssec.wisc.edu/model/nrc/> and http://cimss.ssec.wisc.edu/model/nrc/nrc_tests.html. The web page includes NearCast products discussed in this paper, among others.

References

- Benjamin, Stanley G., & K. J. Brundage, L. L. MoroneL. 1994. The rapid update cycle. part i: Analysis/model description. *Noaa/nws technical procedures bulletin*, **416**, 16.
- Bleck, Rainer. 1973. Numerical forecasting experiments based on the conservation of potential vorticity on isentropic surfaces. *Journal of applied meteorology*, **12**, 737–752.
- Bleck, Rainer. 1978a. On the use of hybrid vertical coordinates in numerical weather prediction models. *Monthly weather review*, **106**, 1233–1244.
- Bleck, Rainer. 1978b. Finite difference equations in generalized vertical coordinates. part i: Total energy conservation. *Contributions to atmospheric physics*, **51**, 360–372.
- Bleck, Rainer, & Benjamin, Stanley G. 1993. Regional weather prediction with a model combining terrain-following and isentropic coordinates. part i: Model description. *Monthly weather review*, **121**, 1770–1785.
- Bleck, Rainer, & Boudra, D. B. 1981. Initial testing of a numerical ocean circulation model using a hybrid (quasi-isopycnic) vertical coordinate. *Journal of physical oceanography*, **11**, 755–790.
- Bolton, David. 1980. The computation of equivalent potential temperature. *Monthly weather review*, **108**, 1046–1053.

- Buzzi, A., & Rizzi, R. 1975. Isentropic analyses of cyclogenesis in the lee of the alps. *Riv. Ital. geofis., act! del xiii collg. intern. meteor., alpillio*, 7–14.
- Byers, Horace. 1938. On the thermodynamic interpretation of isentropic charts. *Monthly weather review*, **66**, 63–68.
- Danielsen, Edwin F. 1959. The laminar structure of the atmosphere and its relation to the concept of a tropopause. *Archiv fur meteorologie, geophysik und bioklimatologie serie a*, **11**, 293–332.
- Danielsen, Edwin F. 1961. Trajectories: Isobaric, isentropic and actual. *Journal of meteorology*, **18**, 479–486.
- Danielsen, Edwin F. 1964. *Project springfield report*. Defense atomic support agency.
- Danielsen, Edwin F. 1966. *Research in four-dimensional diagnosis of cyclonic storm cloud systems*. Tech. rept. Air Force Cambridge Research Labratory. Report Number 66-30.
- Danielsen, Edwin F. 1967. *Moist isentropic flow and trajectories in a developing wave cyclone*. Tech. rept. Air Force Cambridge Research Labratory. Report Number 67-0617.
- Danielsen, Edwin F. 1968. Stratospheric-tropospheric exchange based on radioactivity, ozone and potential vorticity. *Jornal of the atmospheric sciences*, **25**, 502–518.

- Eliassen, Arnt, & Raustein, Elmer. 1968. A numerical integration experiment with a model atmosphere based on isentropic surfaces.
- Greenspan, Donald. 1972. A new explicit discrete mechanics with applications. *J. franklin inst.*, **294**, 231–240.
- Greenspan, Donald. 1973. *Discrete models*. Addison-Wesley.
- Kocin, Paul J., Uccellini, Louis W., & Petersen, Ralph A. 1986. Rapid evolution of a jet streak circulation in a pre-convective environment. *Meteorology and atmospheric physics*, **1986**, 103–138.
- Li, Zhenglong, Li, Jun, Menzel, W. Paul, III, James P. Nelson, Schmit, Timothy J., Weisz, Elisabeth, & Ackerman, Steven A. 2008. Forecasting and nowcasting improvement in cloudy regions with high temporal goes sounder infrared radiance measurements. *Journal of geophysical research*, **114**, 15.
- Library, SSEC. cited 2013. *SSEC satellite meteorology timeline*. [Available online at <http://library.ssec.wisc.edu/timeline/>].
- Montgomery, Raymond B. 1937. A suggested method for representing gradient flow in isentropic surfaces. *Bulletin of the american meteorological society*, **18**, 210–212.
- Moore, James T. 1987. Isentropic analysis and interpretation: operational applications to synoptic and mesoscale forecast problems.

- Namias, Jerome. 1939. The use of isentropic analysis in short term forecasting. *Journal of the aeronautical sciences*, **5**, 295–298.
- Neamtan, S. M. 1944. Pressure tendencies and stability changes in an isentropic surface. *Bulletin of the american meteorological society*, **25**, 127–136.
- Oliver, V. J., & Oliver, M. B. 1951. *Compendium of meteorology: Meteorological analysis in the middle latitudes*. American Meteorological Society.
- Petersen, Ralph A., & Uccellini, Louis W. 1979. The computation of isentropic atmospheric trajectories using a 'discrete model' formulation. *Monthly weather review*, **107**, 566–574.
- Petersen, Ralph A., Aune, Robert, Dworak, Richard, & Line, William. 2012. Using analysis of the information content of goes/seviri moisture products to improve very-short-range forecasts of the pre-convective environment. *In: 2012 eumetsat meteorological satellite conference*.
- Petterson, S. 1956. *Weather analysis and forecasting*. 2 edn. Vol. 1. McGraw-Hill.
- Reiter, E. R. 1972. Atmospheric transport processes; part3, hydrodynamic tracers. *Quarterly journal of the royal meteorological society*, 212.
- Rosby, Carl-Gustaf. 1937a. Aerological evidence of large-scale mixing in the atmosphere. *American geophysical union*, **18**, 130–136.

- Rosby, Carl-Gustaf. 1937b. Isentropic analysis. *Bulletin of the american meteorological society*, **18**, 201–209.
- Sechrist, F. S., & Dutton, D. A. 1970. Energy conversions in a developing cyclone. *Monthly weather review*, **98**, 354–362.
- Shaw, Sir Napier. 1933. Manual of meteorology. 259–256.
- Spilhaus, Athelstan F. 1940. The shear-stability ratio vector and its use in isentropic analysis. *Bulletin of the american meteorological society*, **21**, 239–248.
- Staff, Journal. 2011. *Tornado devastates mapleton; only minor injuries reported.*
- Starr, Victor P. 1940. The construction of isentropic relative motion charts. *Bulletin of the american meteorological society*, **21**, 236–239.
- Uccellini, Louis. 1976. Operational diagnostic applications of isentropic analysis. *National weather digest*.
- Wilson, Laurence J. 1985. Isentropic analysis-operational applications and interpretation, third edition. *Atmospheric environment service, canada*, 35.